PAPER

Statistical assessment of ELM triggering by pellets on JET

IOP Publishing | International Atomic Energy Agency Nuclear Fusion

Nucl. Fusion **61** (2021) 036035 (24pp) https://doi.org/10.1088/1741-4326/abd861

Statistical assessment of ELM triggering by pellets on JET

M. Lennholm[1,2,3,*], R. McKean[1], R. Mooney[1], G. Tvalashvili[1], G. Artaserse[1,4], M. Baruzzo[5], E. Belonohy[1], G. Calabro[6], I.S. Carvalho[1,7], C.D. Challis[1], E. de la Luna[8], D. Frigione[4], L. Garzotti[1], R.B. Henriques[1,7], J. Hobirk[9], P. Jaquet[1], A. Kappatou[9], D. Keeling[1], D. King[1], P.T. Lang[9], E. Lerche[10], P.J. Lomas[1], C. Lowry[1], M. Maslov[1], S. Moradi[11], M.F.F. Nave[7], I. Nunes[12], C. Perez von Thun[13], C. Reux[14], F.G. Rimini[1], A.C.C. Sips[2,3], C. Sozzi[15], M. Valovic[1], D. Van Eester[10] and JET contributors[a]

EUROfusion Consortium, JET, Culham Science Centre, Abingdon, OX14 3DB, United Kingdom of Great Britain and Northern Ireland

[1] United Kingdom Atomic Energy Authority, Culham Centre for Fusion Energy, Culham Science Centre, Abingdon, Oxon, OX14 3DB, United Kingdom of Great Britain and Northern Ireland

[2] JET Exploitation Unit, Culham Science Centre, Abingdon, OX14 3DB, United Kingdom of Great Britain and Northern Ireland

[3] European Commission, B-1049 Brussels, Belgium

[4] ENEA C.R. Frascati, Roma, Italy

[5] Consorzio RFX, Corso Stati Uniti 4, Padova, Italy

[6] Department of Economics, Engineering, Society and Business Organization (DEIm), University of Tuscia, Largo dell'Università snc, 01100 Viterbo, Italy

[7] Instituto de Plasmas e Fusão Nuclear, Instituto Superior Técnico, Universidade de Lisboa, Lisboa, Portugal

[8] Laboratorio Nacional de Fusión, CIEMAT, 28040, Madrid, Spain

[9] Max-Planck-Institut für Plasmaphysik, D-85748 Garching, Germany

[10] LPP-ERM/KMS, EUROfusion Consortium Member, TEC, Brussels, Belgium

[11] Fluid and Plasma Dynamics, ULB, Campus Plaine, CP 231 Boulevard du Triomphe, 1050 Bruxelles, Belgium

[12] ITER Organization, Route de Vinon-sur-Verdon, CS 90 046, 13067 Saint-Paul-lez-Durance Cedex, France

[13] Institute of Plasma Physics and Laser Microfusion, 23 Hery Street, 01-497 Warsaw, Poland

[14] CEA, IRFM, F-13108 Saint-Paul-lez-Durance, France

[15] National Research Council, Institute for Plasma Science and Technology (CNR-ISTP), via R.Cozzi 53, Milano 20125, Italy

E-mail: morten.lennholm@jet.uk

Received 19 September 2020, revised 9 December 2020
Accepted for publication 5 January 2021
Published 22 February 2021

Abstract

This article investigates the triggering of ELMs on JET by injection of frozen pellets of isotopes of Hydrogen. A method is established to determine the probability that a specific pellet triggers a particular ELM. This method allows clear distinction between pellet-ELM pairs that are very likely to represent triggering events and pairs that are very unlikely to represent such an event. Based on this, the pellet parameters that are most likely to affect the ability of pellets to trigger ELMs have been investigated. It has been found that the injection location is very important, with injection from the vertical high field side showing a much higher triggering efficiency than low field side (LFS) injection. The dependence on parameters such as pellet speed and size and the time since the last ELM is also seen to be much stronger

[*] Author to whom any correspondence should be addressed.

[a] See Joffrin *et al* 2019 (https://doi.org/10.1088/1741-4326/ab2276) for the JET team.

for LFS injection. Finally, the paper illustrates how improvements to the pellet injection system by streamlining the pellet flight lines and slightly increasing the pellet size has resulted in a significantly improved ability to deliver pellets to the plasma and trigger ELMs.

Keywords: tokamaks, ELMs, pellets, ELM triggering

(Some figures may appear in colour only in the online journal)

1. Introduction

The aim of current tokamaks is to pave the way for larger future devices such as ITER, eventually allowing the construction of power producing nuclear fusion reactors. This aim means that it is essential that current devices demonstrate high performance which remain stable for significant durations. The most promising scenarios to achieve this goal, and the reference scenarios for ITER operation, are ELMy H-mode scenarios [1–3]. One of the main challenges facing current machines aiming to achieve steady high performance is the control of the ELM activity. Too infrequent, and hence too large, ELMs are likely to cause significant damage to the plasma facing components. In machines with all metal walls such as ASDEX-Upgrade and JET, a further complication is added. Here it is observed that, if the ELM frequency becomes too low, the plasma rapidly becomes polluted by high-Z metallic impurities and this regularly causes the plasma to disrupt [4–7]. On these machines it is therefore essential to keep the ELM frequency sufficiently high. On JET, the simplest way to maintain a sufficiently high ELM frequency is to inject a rather large continuous gas flow into the vacuum vessel. Unfortunately, nothing comes without a price and increasing gas injection leads to a significant reduction of the plasma confinement and hence of the fusion performance which can be achieved. Using gas to control the ELM frequency, JET tends to walk close to the edge of runaway impurity accumulation, trying to maintain sufficient ELM frequency with the lowest possible gas injection rate. A feedback controller has been developed to maintain the ELM frequency as desired by varying the gas injection in real time [8]. This allows JET to run close to the edge without falling off too often. Significant levels of gas still have to be injected to maintain this minimum ELM frequency leading to reduced performance. It is therefore desirable to find alternative ways to maintain a sufficiently high ELM frequency. One way of triggering ELMs, which is used on JET, is so-called vertical kicks. This method uses a rapid change in the radial magnetic field, which provokes a rapid vertical plasma movement, to induce ELMs. The kicks risk inducing a vertical displacement event followed by a large disruption, potentially causing damage to the machine. For this reason, vertical kicks cannot be used at high plasma current [9–11]. A more promising way of controlling ELMs is the injection of small pellets of frozen hydrogenic isotopes into the plasma. Such pellets have been seen to be able to trigger ELMs and the hope is that the ELM frequency can be maintained at the desired level with minimum gas injection and minimum reduction of the confinement. On ITER, neither gas injection nor vertical kicks, are options for ELM control and hence ITER scenarios will be relying on pellet injection and/or resonant magnetic perturbations to control or suppress the ELMs [12, 13]. Experiments with pellets have been performed on various tokamaks for ELM control and fuelling [14–19]. On DIII-D the influence of the main pellet parameters on ELM triggering has been investigated. Here pellets have been injected from various locations and with a range of sizes and speeds [16]. These experiments showed that the fuelling efficiency increased strongly when the pellets were launched from the high field side (HFS) as compared to the fuelling with pellets launched from the low field side (LFS). Simulations with the JOREK code have investigated the ELM triggering dependence of launch location, pellet mass and speed [20–22] as described below. In the following a statistical analysis of the parametric dependence of ELM triggering by pellets on JET is presented.

JET is equipped with a high frequency pellet injector and this has been operational over the last 10 years [11, 23–25]. The pellets injected by this system, do not arrive at the plasma at constant intervals. This is mainly due to the fact that they have to travel $\sim$10 m through a pipe before arriving in the plasma and that they do not all leave the injector with the same speed. Though significant improvements in the plasma performance has been achieved using this pellet injector, the scattered way in which the pellets arrive at the plasma means that the ELMs generated are a mixture of spontaneous and triggered ELMs. As a result, it is difficult to assess how different properties of the pellets govern their ability to trigger ELMs and to investigate the differences between triggered and spontaneous ELMs. The aim of this paper is threefold: (1) to develop a method to ascertain which pellets trigger ELMs and which ELMs are triggered. As this cannot be done with 100% accuracy, the method described below gives the probability that, given a pellet-ELM pair, the former triggers the latter. (2) To determine which fraction of the launched pellets reach the plasma and where the rest of the pellets are lost. (3) For the pellets arriving in the plasma, to investigate the influence of the main pellet parameters on the ability of the pellets to trigger ELMs. The main pellet parameters investigated are (i) pellet injection location, (ii) pellet size and (iii) pellet speed.

The analysis is based on a database containing the majority of pellets injected into ELMy H-mode plasmas in JET since the installation of the new ITER like wall in 2011. The main engineering parameters for the plasmas included vary widely within this database. The range of

variation of these parameters is as follows: plasma current: 1.5–3.8 MA, toroidal field: 2.0–3.4 T, neutral beam heating power 9–32 MW, deuterium gas injection rate: $0–1 \times 10^{23}$ electrons/s.

The paper is organised as follows: section 2 looks at the current understanding of the physics behind the occurrence of ELMs and how external perturbations can affect the ELM cycle. Section 3 gives an overview of the JET pellet injection system and the evolution it has undergone since it is installation in 2007. In section 4, a Bayesian analysis of the pellet and ELM time sequences is presented, and a probability is ascribed to each pellet and each ELM of triggering and being triggered respectively. In section 5, a similar method is used to track pellets on their journey from launch by the injector, through the flight line transit system to the plasma. This allows the determination of the velocity of the pellets at the time they arrive in the plasma. This section also attempts to assess where pellets are lost along the flight line. Section 6 analyses the main parameters which affect the ability of pellets to trigger ELMs and section 7 discusses how the observations can be tied into the current physics understanding as described in section 2. Finally, conclusions are drawn in section 8.

2. Natural and triggered ELMs

Recent simulations with the JOREK code, simulating more than one ELM period, indicate that the ELM occurs when several MHD modes with different toroidal mode numbers interact non-linearly, eventually leading to explosive growth of these modes [26]. These simulations show that such modes will already exist, with a not insignificant amplitude, just after an ELM has occurred. The larger these 'seed' modes are, just after an ELM, the sooner the next ELM will occur. Thus, the characteristics of the ELMs themselves can influence the ELM frequency. Experimental investigations of the modes involved in this nonlinear mode coupling have shown that, when such modes are present, a small perturbation may provoke the explosive growth significantly earlier than this would have happened in the absence of such a perturbation [27]. This picture extends the traditional image of peeling–ballooning stability, where a stability boundary exists in edge pressure gradient—edge current space and where an ELM occurs when this boundary is crossed. According to this recent research, small perturbations may be used to trigger ELMs, under the right conditions, thereby significantly increasing the ELM frequency. According to this mechanism 'seed' modes of finite amplitude are required for the triggering of an ELM. The closer the plasma, in terms of edge pressure gradient and edge current, gets to the stability boundary, the smaller the required seed modes. In this picture the stability boundary is given by the point where noise is enough to trigger the ELM. The perturbations investigated in this article are the perturbations resulting from the injection of small pellets into the plasma. The toroidal asymmetry of the pellet perturbation can introduce seed modes in the sense just described. The expected effect of injecting pellets from different locations and with different sizes and speeds has been investigated using the JOREK code [21]. In these investigations it was found that ELMs could be triggered further from the instability limit when the size of the pellets increased. This is readily understood from the above picture, as larger pellets cause a larger change in edge parameters and a larger non axisymmetric perturbation leading to larger seed modes. The expected evolution of these modes can be seen from [21]. Similarly, the ELM triggering probability would be expected to increase with increased pellet speed as faster pellet would penetrate further into the plasma edge. Furthermore, it was found that ELM triggering would be expected to be easier with HFS launch than with LFS launch. The explanation of this is that the natural pellet drift direction on the HFS is towards the plasma centre, whereas this direction is away from the plasma on the LFS. As a consequence, a larger and deeper perturbation can be achieved with HFS launch than LFS launch, assuming similar pellet size and velocity. The direction of the pellet drift is the main reason that plasma fuelling would preferably use HFS launch. For ELM triggering, on the other hand, LFS launch may be preferable if it is desirable to be able to trigger ELMs with minimal fuelling, as LFS launch would fuel much less for the same pellet properties. This may be offset by the fact that LFS launch would be expected to require larger and/or faster pellets to allow ELM triggering, at which point the fuelling may become similar to the fuelling resulting from smaller pellets injected from the HFS.

The aim of this paper is to investigate whether the expectations based on JOREK simulations outlined above can be confirmed through a statistical analysis of a large database of pellets injected into JET ELMy H-mode plasmas.

3. Evolution of the JET pellet injection system

The JET pellet injector, installed in 2007, can inject hydrogen or deuterium pellets in two distinct size ranges, fuelling pellets and (ELM) pacing pellets [23–25]. For deuterium fuelling pellets the size range is 8–12 mg. For pacing pellets, the size range was increased in 2017 (from shot 93 000 onwards) to improve the pellet survivability. The deuterium pacing pellet size range was 0.47–0.69 mg before 2017 and 0.86–1.23 mg thereafter. The JET pellet injector, manufactured by PELIN, is based on pneumatic propulsion, where the pellets are fired into the flight tube by compressed helium. The result of this is that the pellet velocity varies significantly from pellet to pellet, in contrast to the behaviour of pellets injected using a pellet centrifuge [14, 15]. In order to achieve frequencies for pacing pellets up to 50 Hz, the injector uses two separate barrels from which pacing pellets are fired alternately. For fuelling pellets, a single larger barrel is used with the fuelling pellet frequency limited to 15 Hz. The following analysis is based solely on pacing pellets.

The pellets have been injected into JET from two different locations, one equatorially through an outboard horizontal port (LFS injection) and one from the inboard side injecting near the top of the machine (vertical high field side (VHFS) injection). Originally it was possible to switch between these two injection locations, but the VHFS injection line was too tortuous and hence very few of the pacing pellets could

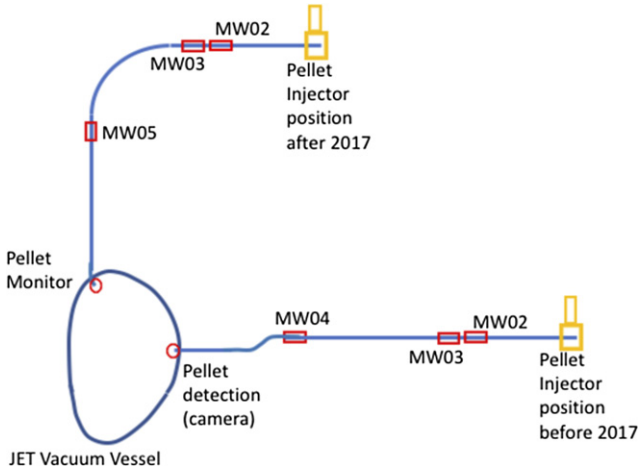

Figure 1. Pellet injection geometries and the location of the detectors which observe the pellets for the two different injector locations—pre- and post-2017.

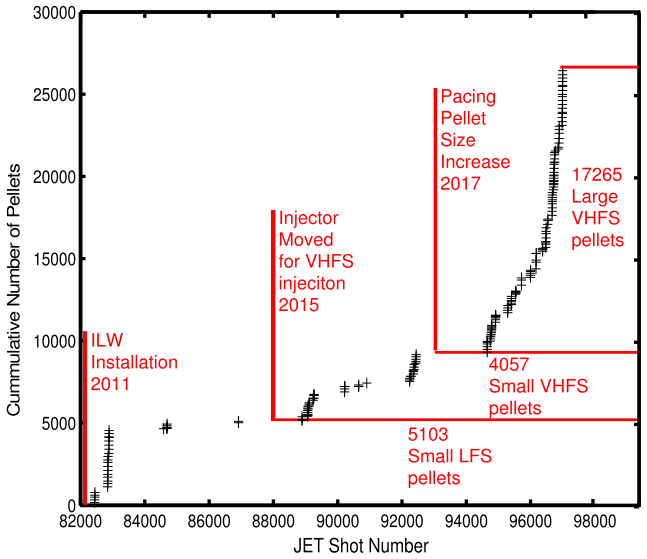

Figure 2. Cumulative numbers of pellets injected into JET ELMy H-modes and used in this analysis. Each cross corresponds to a JET shot. The times when the system was modified are indicated.

survive injection through this line. The few pacing pellets that did survive were, however, sufficient to indicate that VHFS injection was likely to be much more effective at ELM pacing than LFS injection. For this reason, the pellet injector was moved in 2015 to a location at the top of the JET machine, abandoning LFS injection but allowing VHFS injection via a much simpler, shorter, flight path, with fewer free transit sections and less severe bends. As a consequence, all discharges executed before 2015 (shot numbers $<$88 000) included in this analysis use LFS injection, while all later discharges use VHFS injection. Figure 1 shows the two injection layouts. The figure also shows the locations of the detectors, appearing as free flight transit sections for the pellets, which allow observation of the pellets as they travel through the flight line before arriving in the vacuum vessel.

To select the data used for the statistical analysis presented in this paper, the following criteria have been used. Time windows are determined by (i) the plasma being in H-mode with distinct type 1 or compound ELMs and (ii) the pellet injector operating well, launching deuterium pacing pellets throughout the time window. Though selection of the time windows used for the analysis is somewhat subjective, this analysis includes the vast majority of pacing pellets injected into steady ELMy H-modes. Figure 2 shows the cumulative number of pellets used in the analysis as a function of JET shot number. Vertical lines show the time when the injector was moved and when the pacing pellet size was increased respectively and horizontal lines show the number of pellets up until these times, with the number of pellets for each of the three time periods given in the figure. Thus, the analysis involves a total of 26 425 pellets from 205 different JET discharges, distributed as follows:

(a) 5103 small pacing pellets from 31 discharges with injection from the LFS,
(b) 4057 small pacing pellets from 52 discharges with injection from the VHFS
(c) 17 265 large pacing pellets from 122 discharges with injection from the VHFS

The improved performance associated with the move to VHFS injection and thereafter with the increase of the pacing pellet size, has rendered pellet injection increasingly valuable for ELM control and, as can be seen from figure 2, the use of pellets has become significantly more prevalent as a consequence of these improvements. Currently pellet injection is an integral part of developing the ‘baseline scenario’, which is one of the main high-performance scenarios being developed for the upcoming JET deuterium tritium experiments [1, 2]. The use of pellet injection in various operations scenarios on JET has been analysed and described in the following papers [28–30].

The pellets are observed by a number of microwave cavities (MW0x) in their passage through the flight line, as indicated in figure 1. MW02 and MW03 are located close together and close to the pellet launch location. MW02 is tuned to observe pacing pellets, while MW03 is tuned for fuelling pellets. Though MW03 was not able to detect the pacing pellets before the increase of the size in 2017, it is able to see most pacing pellets after this increase. MW04, tuned for pacing pellets, was, until it is removal in 2015, located near the entry into the vacuum vessel in the LFS injection line, while MW05, tuned for fuelling pellets is located near the entry into the vacuum vessel in the VHFS injection line. MW05 has been calibrated to be able to see smaller pellets than it was originally intended for and hence it could, as opposed to MW03, see most of the pacing pellets even before the size increase.

As stated in the introduction, the aim of this paper is to determine the probability of a pellet triggering an ELM as a function of the main pellet parameters; pellet injection location, pellet size and pellet speed. The analysis performed only considers deuterium pacing pellets.

Before proceeding to investigate these probabilities, it is essential to have a clear way of determining whether an ELM is triggered or not and whether a pellet is 'triggering' or not. To this purpose a Bayesian technique is developed which, for each pellet–ELM pair, ascribes a probability that the pellet has triggered said ELM. Further analysis can then either be weighted by this probability or pellet-ELM pairs with intermediate probabilities can be eliminated from the analysis to compare only clear triggering and clear non-triggering events. The method developed is generic and can be used to determine 'correlation probabilities' of any two series of discrete events. This methodology is also used to determine the speed of the injected pellets by allowing the identification of individual pellets as they pass the various detectors placed along their flight path through the injection pipe.

4. Correlation of pellet and ELM sequences

A typical discharge, where pacing pellets are injected through the VHFS flight line into an ELMy H-mode plasma, is shown in figure 3. The top three boxes show the pellet request and the signals from the detectors along the flight path. The signals from MW02 and MW05 give the mass of the pellet as it moves through these detectors. The amplitude of the signal from the monitor looking at the pellets as they enter the vacuum vessel is, however, not very well correlated with the pellet sizes as the signal depends strongly on the angle at which the pellet exits the flight tube. This angle varies so much that about 10%–20% of pellets exiting the flight tube are not seen by the monitor at all. Only pellets giving a signal in the monitor exceeding a fixed threshold, are considered for the following analysis of pellet–ELM correlation and for the parametric dependence of ELM triggering probabilities. The 4th box shows the signature of ELMs as seen in a divertor spectroscopy beryllium line. An ELMs is considered to have occurred when the derivative of the spectroscopy exceeds a certain threshold. The final box shows the heating powers. The thresholds used for the detection of pellets and ELMs as described, are clearly a question of individual judgement. For ELMs, these thresholds have been chosen to give a detection which agrees well with what would be deemed ELMs by inspection of numerous individual ELMs. In this inspection the agreement with the observation of ELM signatures in other signals, such as the total radiated power measured by the JET bolometer, has been considered. This being said, there are clearly some ELM like signatures which are too small to be qualified as ELMs according to this criteria. Likewise, there are signatures in the pellet monitor, which are deemed too small to be considered pellets for the purpose of this analysis. Thus, the analysis concentrates on the correlation between clear pellets and clear ELMs. Before proceeding to analyse the correlation between the ELM and monitor signals, individual ELMs and pellets detected in these signals are used to generate two time sequences. The analogue ELM and pellet signals are shown in the first two boxes in figure 4, while those at the bottom box shows the two time sequences as determined using the described criteria. Thus, we have a time sequence for pellets arriving in

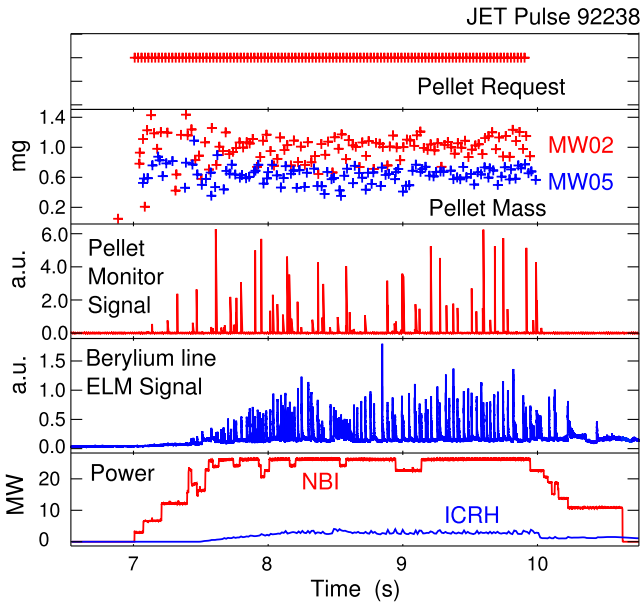

Figure 3. Typical discharge with pellet injection from the VHFS line. The figure shows, from top to bottom, pellet requests, pellet mass in microwave cavities, pellet monitor signal, ELM signal and heating power.

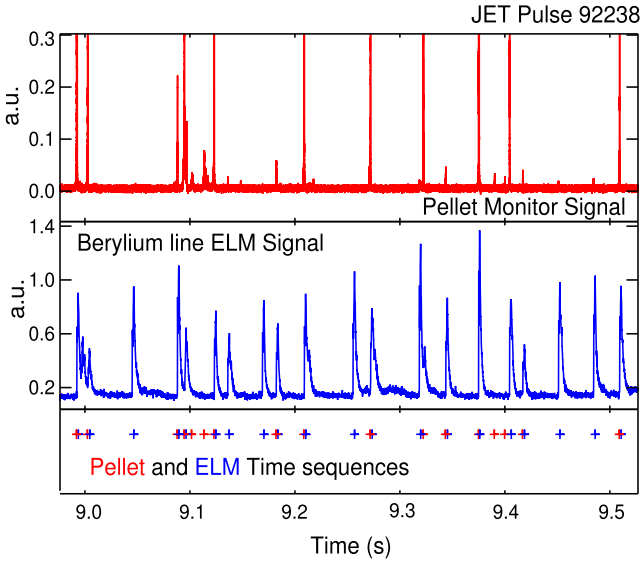

Figure 4. Zoom in on a short time interval showing the pellet monitor signal, the ELM signal and the two time sequences of the detected pellets and ELMs.

the plasma:

$$S_{\mathrm{P}} = [t_{\mathrm{P1}}\ t_{\mathrm{P2}} \ldots\ldots t_{\mathrm{P}n}] \tag{1}$$

and a time sequence for ELMs:

$$S_{\mathrm{E}} = [t_{\mathrm{E1}}\ t_{\mathrm{E2}} \ldots\ldots t_{\mathrm{E}m}]\,. \tag{2}$$

The following analysis can be used to investigate the correlation between any such pairs of time sequences. The first step is to create the difference matrix which includes the time difference between all pairs of times from the two sequences

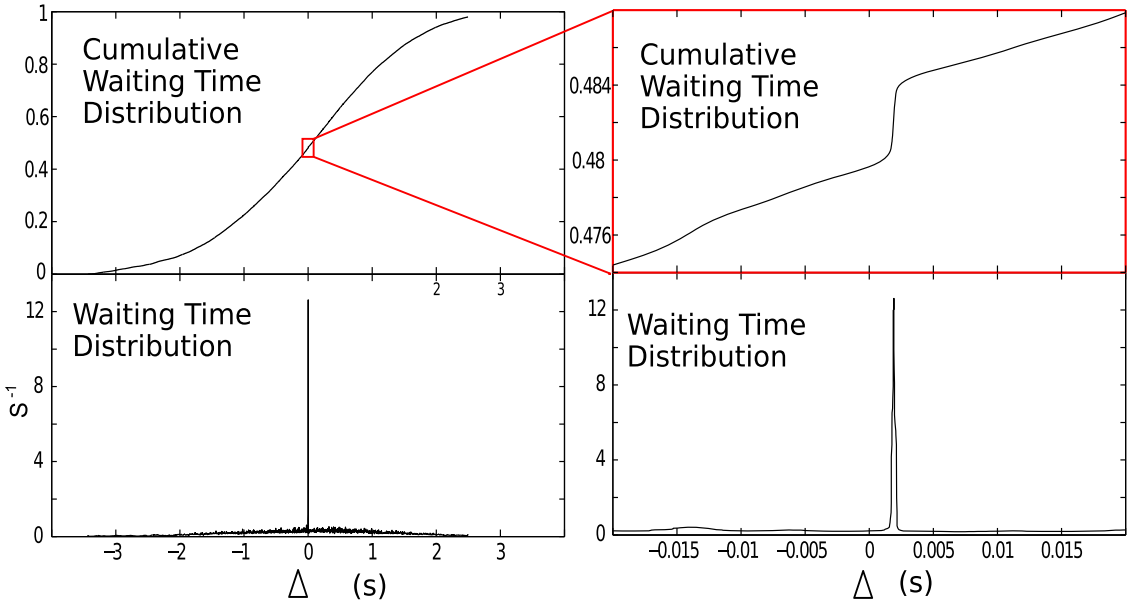

Figure 5. Waiting time distributions between pellets and ELMs: (top left graph) cumulative distribution $C(\Delta)$. (Bottom left graph) distribution $D(\Delta)$. (Right top and bottom graphs) zoom around 0 ms.

$\Delta_{kl} = t_{El} - t_{Pk}$ as follows

$$M_{\mathrm{PE}} = \begin{bmatrix} \Delta_{11} & \cdots & \Delta_{m1} \\ \vdots & \ddots & \vdots \\ \Delta_{1n} & \cdots & \Delta_{mn} \end{bmatrix}. \tag{3}$$

Taking all the elements in this matrix and sorting them we can get an ordered series of time differences as follows:

$$S_\Delta = \left[\Delta_{o1}\ \Delta_{o2} \ldots \Delta_{op} \ldots \Delta_{oh}\right] \quad \text{where}$$
$$\Delta_{o1} \leqslant \Delta_{o2} \ldots \leqslant \Delta_{op} \leqslant \ldots \leqslant \Delta_{oh}. \tag{4}$$

Here Δ_{o1} and Δ_{oh} are the smallest and largest elements of M_{PE} and $h = mn$. Note that the values of Δ_{op} can be positive or negative.

Based on S_Δ the cumulative distribution of waiting times between pellets and ELMs can be constructed: $C\left(\Delta_{op}\right) = \frac{p}{h}$ where p goes from 1 to h. From this the waiting time distribution $D(\Delta)$ can be found by differentiating C with respect to Δ:

$$D(\Delta) = C'(\Delta). \tag{5}$$

In order for the differentiation not to generate a very noisy signal some smoothing of $C(\Delta)$ is required.

Figure 5 shows $C(\Delta)$ and $D(\Delta)$ for the discharge in figure 3. The general cumulative distribution in the top left box of figure 5 does not immediately seem to have any significant features, but the derivative shown in the bottom left box shows a very sharp spike near 0. The top and bottom right boxes in this figure shows a zoom around the area where the spike occurs, and it is clear that there is a very significant number of waiting times which fall in a very small interval around 2 ms.

This method would work even if the correlation between the two time series does not link a point from the first series with the nearest subsequent point from the second series. This feature will become important in section 3, but for the correlation between pellets seen in the monitor signal and ELMs, the analysis can be simplified by looking only at the previous pellet for each ELM. This is achieved by reducing M_{PE} to a $1 \times m$ matrix by selecting the smallest positive Δ in each column of M_{PE}. This gives the following sequence:

$$S_{\mathrm{PE}} = \left[\Delta_{1\mathrm{minpos}}\ \Delta_{2\mathrm{minpos}} \ldots \Delta_{m\mathrm{minpos}}\right]. \tag{6}$$

A number of discharges can be incorporated in the analysis to improve the statistics. With the data reduction achieved in (6) including all relevant discharges becomes manageable. From the distribution in figure 5, we can deduce that pellet-ELM pairs, where the time difference between pellet and ELM time points is in the range of the peak of the distribution, are likely to indicate that the pellet triggers the ELM.

As natural ELMs do not occur with high regularity and as the JET pellets do not enter the plasma at regular intervals, there is a finite probability that an ELM which occurs within the peak occurs naturally rather than being triggered. To be able to state the likelihood of an ELM being triggered by a specific pellet, a statistical method is employed to ascribe a value to each ELM giving the probability that this ELM is a triggered ELM. In order to do this, we need to know how probable it is that a natural ELM arrives at time Δ after a pellet. We define this probability as $D_N(\Delta)$. To estimate $D_N(\Delta)$ from the data we introduce an evenly spaced array of time points

$$S_N = [t_{\mathrm{s}}\ t_{\mathrm{s}} + \mathrm{d}t\ t_{\mathrm{s}} + 2\mathrm{d}t \ldots\ldots t_{\mathrm{s}} + K\mathrm{d}t], \tag{7}$$

where $\mathrm{d}t$ is much smaller than the average pellet and ELM intervals and t_{s} is an arbitrarily selected time with $t_{\mathrm{s}} < t_{\mathrm{P1}}$ and $t_{\mathrm{s}} < t_{\mathrm{E1}}$. Similarly K is chosen such that $t_{\mathrm{P}n} < t_{\mathrm{s}} + K\mathrm{d}t$ and $t_{\mathrm{E}m} < t_{\mathrm{s}} + K\mathrm{d}t$. Replacing S_{P} from equation (1) by S_N from equation (7) the analysis can be repeated. The top box of figure 6 shows $C(\Delta)$ and $C_N(\Delta)$ where $C_N(\Delta_0) =$

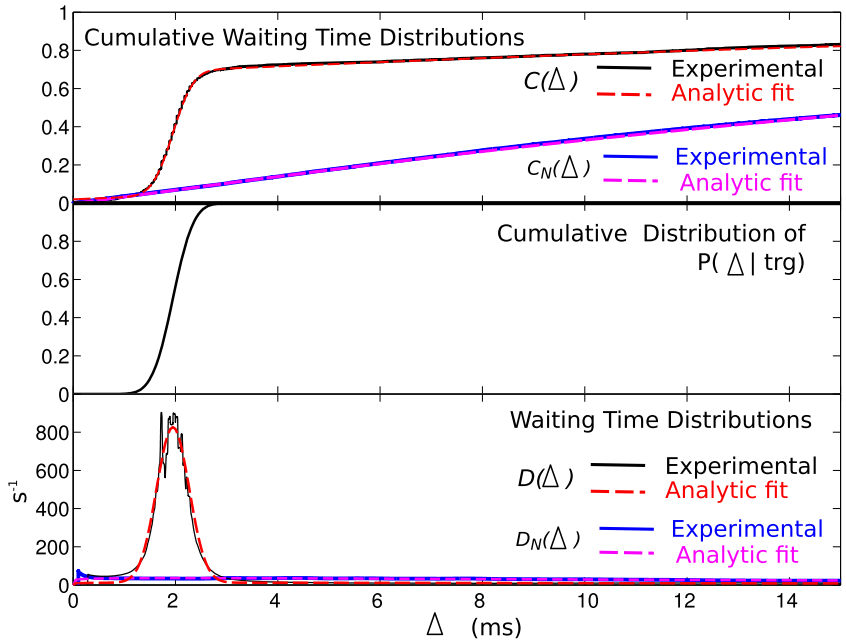

Figure 6. Waiting time distributions between pellets and ELMs and between random time points and ELMs: (top graph) cumulative distributions $\int_0^{\Delta_0} P(\Delta)\,\mathrm{d}\Delta$ (red and black) and $\int_0^{\Delta_0} P\left(\Delta|\overline{\mathrm{trg}}\right)\mathrm{d}\Delta$ (blue and magenta). (Middle graph) $\int_0^{\Delta_0} P\left(\Delta|\mathrm{trg}\right)\mathrm{d}\Delta$. (Bottom graph) Distributions $P(\Delta)$ (red and black) and $P\left(\Delta|\overline{\mathrm{trg}}\right)$ (blue and magenta). The analytic fits to the measured data are the dashed red and magenta lines. A very good fit is achieved.

$\int_0^{\Delta_0} D_N(\Delta)\,d\Delta$ is the cumulative distribution of the waiting time to the next ELM from a random point in time. Notice that both triggered and non-triggered ELMs are considered here. This is justified, as one has to assume, apriori, that we do not know which ELMs are triggered. If ELMs considered to be triggered are subsequently eliminated in this analysis the effect on the derived cumulative distribution function $C_N(\Delta)$ is insignificant in terms of the further analysis. To progress the analysis, we exploit the following Bayesian equation:

$$P(\Delta) = P(\mathrm{trg}) \cdot P\left(\Delta|\mathrm{trg}\right) + P\left(\overline{\mathrm{trg}}\right) \cdot P\left(\Delta|\overline{\mathrm{trg}}\right). \quad (8)$$

Here $P(\mathrm{trg})$ is the probability that an ELM is triggered, $P\left(\overline{\mathrm{trg}}\right)$ is the probability that an ELM is not triggered, $P(\Delta)$ is the probability that an ELM occurs after a waiting time of Δ. $P\left(\Delta|\mathrm{trg}\right)$and $P\left(\Delta|\overline{\mathrm{trg}}\right)$ are the conditional probabilities of an ELM occurring after a waiting time of Δ under the conditions that this ELM is triggered and not triggered respectively. Integrating (8) we can derive the cumulative version of this equation:

$$\int_0^{\Delta_0} P(\Delta)\,\mathrm{d}\Delta = P(\mathrm{trg}) \cdot \int_0^{\Delta_0} P\left(\Delta|\mathrm{trg}\right)\mathrm{d}\Delta + P\left(\overline{\mathrm{trg}}\right) \cdot \int_0^{\Delta_0} P\left(\Delta|\overline{\mathrm{trg}}\right)\mathrm{d}\Delta. \quad (9)$$

We can now identify elements in this equation with the traces of the observed cumulative distributions seen in the top box of figure 6. The red/black trace $C(\Delta)$ is the total cumulative waiting time distribution, while the blue–magenta trace $C_N(\Delta)$ is the cumulative waiting time distribution for non-triggered ELMs. Thus:

$$C(\Delta) = \int_0^{\Delta_0} P(\Delta)\,\mathrm{d}\Delta \quad (10)$$

$$C_N(\Delta) = \int_0^{\Delta_0} P\left(\Delta|\overline{\mathrm{trg}}\right)\mathrm{d}\Delta. \quad (11)$$

With this identification it is now possible to find $P(\Delta)$ and $P\left(\Delta|\overline{\mathrm{trg}}\right)$ by taking derivatives. The bottom box in figure 6 shows the resulting distributions with some smoothing applied.

To allow a better analysis it is desirable to approximate the observed distributions by analytic functions. For this purpose, $P\left(\Delta|\overline{\mathrm{trg}}\right)$ is assumed to be a modified waiting time distribution. A standard waiting time distribution would be appropriate under the assumption, that the waiting time from a random point in time until a natural ELM occurs, is independent of any history before this random point in time. The modification to the distribution is introduced to compensate for the fact that this is not true as the ELM period is not fully random, though there is a large variability in this period. The modification is introduced to achieve the best match to the observed distribution function. The distribution of waiting times between pellets and triggered ELMs $P\left(\Delta|\mathrm{trg}\right)$ is assumed to be a normal distribution with the variability of the distribution being dominated by signal noise in the measured data introducing a random variation in the time when the detection thresholds for the two events is passed. The two distributions are as follows:

$$P\left(\Delta|\overline{\mathrm{trg}}\right) = \frac{x}{\Delta_{nt}} \mathrm{e}^{-\frac{\Delta}{\Delta_{nt}}} \cdot \left(1 - \mathrm{e}^{-\frac{\Delta}{\Delta_{nt}}}\right)^{x-1} \quad (12)$$

$$P\left(\Delta|\mathrm{trg}\right) = \frac{1}{\sqrt{\pi}\Delta_w} \mathrm{e}^{-\left(\frac{\Delta-\Delta_m}{\Delta_w}\right)^2}. \quad (13)$$

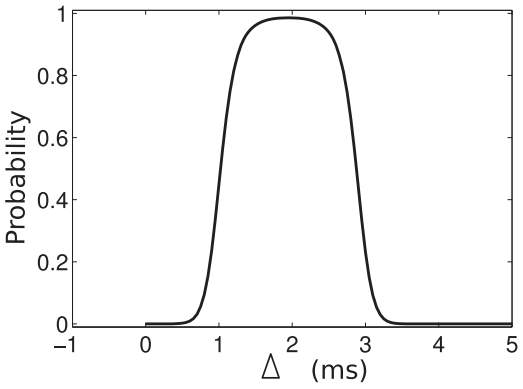

Figure 7. Function giving the probability that an ELM, which is seen at time Δ after a pellet is observed by the pellet monitor, is a triggered by the pellet in question.

Here Δ_{nt} and x are the parameters defining the waiting time distribution while Δ_m and Δ_w are the mean and the width of the normal distribution. Integrating (12) and (13) the analytical cumulative distributions can be found

$$\int_0^{\Delta_0} P\left(\Delta|\overline{\text{trg}}\right) \mathrm{d}\Delta = \left(1 - \mathrm{e}^{-\frac{\Delta}{\Delta_{nt}}}\right)^x \tag{14}$$

$$\int_0^{\Delta_0} P\left(\Delta|\text{trg}\right) \mathrm{d}\Delta = \frac{1}{2}\left(1 - \text{Erf}\left(\frac{\Delta_0 - \Delta_m}{\Delta_w}\right)\right). \tag{15}$$

A good fit with the measured cumulative distributions can be achieved by selecting an appropriate value for $P(\text{trg})$ and for the parameters in equations (14) and (15) and then using (8) to determine $P(\Delta)$. The analytical distributions determined in this way are overlaid on the measured distributions in the top and bottom boxes in figure 6. The analytical distribution for $\int_0^{\Delta_0} P\left(\Delta|\text{trg}\right) \mathrm{d}\Delta$ is shown in the middle box of figure 6.

As a final step we would like to determine the probability that an ELM is triggered if we know that it occurs a time Δ after a pellet is seen in the pellet monitor. In other words, we want to find $P\left(\text{trg}|\Delta\right)$. To achieve this, we use the following Bayesian theorem:

$$P\left(\text{trg}|\Delta\right) = \frac{P(\text{trg}) \cdot P\left(\Delta|\text{trg}\right)}{P(\text{trg}) \cdot P\left(\Delta|\text{trg}\right) + P\left(\overline{\text{trg}}\right) \cdot P\left(\Delta|\overline{\text{trg}}\right)} \tag{16}$$

together with the fact that $P\left(\overline{\text{trg}}\right) = 1 - P(\text{trg})$. Inserting $P\left(\Delta|\text{trg}\right)$ and $P\left(\Delta|\overline{\text{trg}}\right)$ from (12) and (13) with the parameter values found above ($\Delta_{nt} = 22$ ms, $\Delta_m = 1.95$ ms, $\Delta_w = 0.45$ ms and $x = 1.1$) together with $P(\text{trg}) = 0.65$ the dependence seen in figure 7 is found. Figure 7 shows that a very clear distinction can be made between ELMs which are almost certainly triggered and ELMs which are very unlikely to be triggered. This in turn makes it easier to get clear results when looking for differences between triggered and non-triggered ELMs and between triggering and non-triggering pellets.

There is, however, a caveat to this. As mentioned in the introduction, the pellet monitor, which looks at pellets arriving through the VHFS flight line, misses a not insignificant fraction of these pellets. Hence there is likely to be a number of ELMs which are triggered, despite the function in figure 7 showing a very low probability of them being triggered. To get a better understanding of this, one can try to use the above method to correlate pellets seen in the microwave detector situated just outside the vacuum vessel, with ELMs. Attempting to do this does, however, not show any clear correlation due to the large scatter in pellet velocities and hence in flight times between the microwave detector in question and the plasma. One way to improve this, is to determine the velocity of individual pellets as they go through the microwave detector and then predict their arrival time in the plasma. If the correlation method described above, is now applied between these predicted pellet arrival times and the ELMs a better correlation can be found allowing a probability of ELM being triggered to be given even when a triggering pellet is not seen in the pellet monitor. This way ELMs which are unlikely to be triggered can be found with better confidence allowing a more robust statistical comparison between triggered and non-triggered ELMs. We will return to a more quantitative analysis of triggering by pellets not seen in the monitor at the end of the next section which deals with the tracing of pellets through the flight line and the determination of pellet speeds at different points along the injection trajectory.

5. Pellet tracing and pellet survival

To find the velocity of a pellet as it moves through the flight line, it is necessary to determine the times when this specific pellet is seen at consecutive measurement points. This is not straight forward as it is easy to confuse one pellet with another which arrives slightly earlier or later. To progress with this identification, the method described in section 4 is employed to correlate pellets between the different observation points. In the following, an analysis for VHFS discharges is described. This analysis was repeated for LFS injection, with the only difference being that measurements from MW05 were replaced by measurements from MW04. Figure 8 shows the distributions $C(\Delta)$ and $D(\Delta)$ for the correlation between the pellet launch request signal and the signal from the first microwave cavity (MW02), for the discharge shown in figure 3. The most noticeable difference between figures 8 and 5 is the large number of spikes on $D(\Delta)$ seen in figure 8, where figure 5 showed only 1 spike. This is due to the fact that the two time series used for figure 8 are periodic with the same periodicity. This highlights the problem of pellet identification. Which of the spikes is the correct one to look at? Taking the wrong spike will result in the wrong pellet velocity being found.

Repeating this exercise correlating signals from MW02 and MW05 and from MW05 and the pellet monitor leads to the $D(\Delta)$ traces in figure 9. Though there are still numerous spikes in this figure, one spike is dominant as indicated. Note that in the left graphs of figure 9, this peak is not the one corresponding to the smallest positive value of Δ, indicating that the previous pellet normally arrives in the second microwave cavity after the current pellet has passed the first microwave cavity. Having identified clear dominant peaks allows us to find

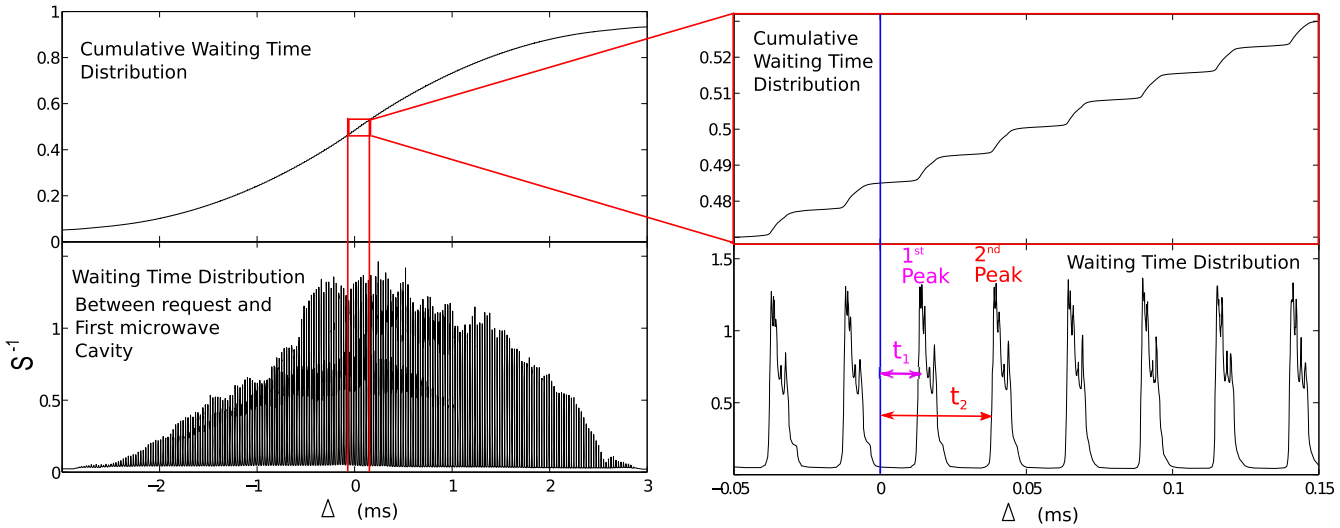

Figure 8. Waiting time distributions between the signal requesting the pellets launch and observation of pellets in the first microwave detector. (Top left graph) Cumulative distribution $C(\Delta)$. (Bottom left graph) Distribution $D(\Delta)$. (Right top and bottom graphs) Zoom around 0 ms.

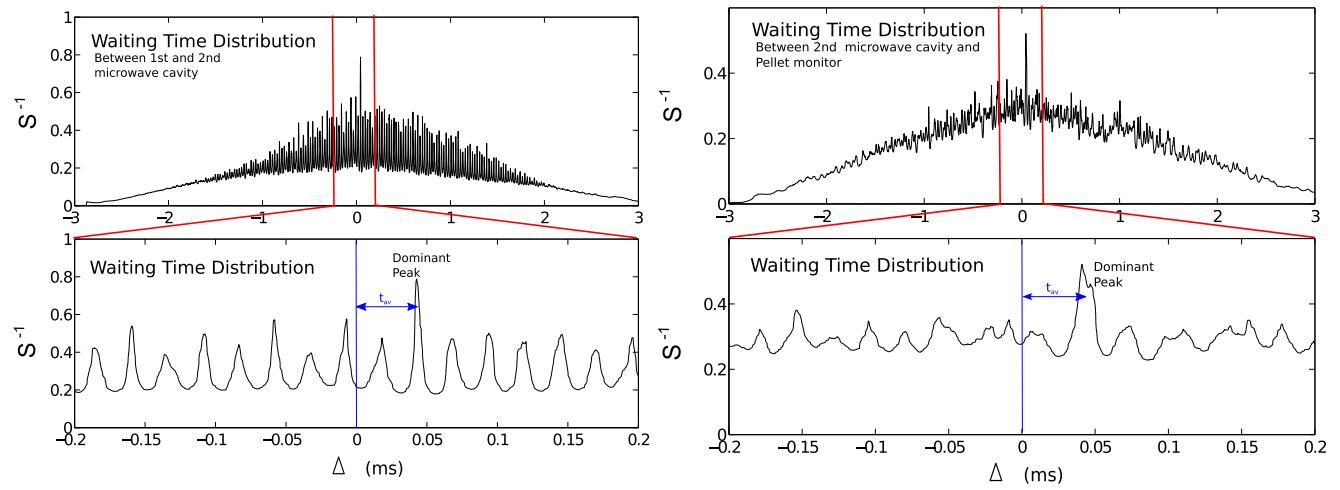

Figure 9. (Left graphs) Waiting time distributions between the 1st and 2nd microwave cavity. (Right graphs) Waiting time distributions between the 2nd microwave cavity and the pellet monitor.

well-defined average times t_{av} taken by pellets to fly between the two microwave cavities and between the second microwave cavity and the pellet monitor respectively as indicated in the figure.

This in turn allows a reasonably robust identification of individual pellets at consecutive observation points and, using the distance between the observation points, the speed of individual pellets can be determined. In a similar way a speed, as determined from the request signal and the MW02 signal, can be found for each of the peaks in figure 8. Figure 10 shows the speed measured between MW02 and MW05 as a function of the speed between the injector and MW02 as found based on either the first (magenta o) or the second (red +) peak in figure 8. A dependence which looks linear is seen for both choices, but neither of the lines describing this dependence pass through the origin as would be expected. The only way to resolve this is to introduce the, reasonable, assumption that there is a delay between a pellet request and the actual launch of the pellet. Adjusting this delay to assure that the resulting velocities fall on a straight line going through the origin, one finds the dependence between velocities given by the blue crosses in figure 10. The delay found in this way is 22 ms. Based on this assumption, the curves described by the red and magenta points in figure 10 would not be expected to fall on straight lines but on curves which pass through the origin. This non-linearity is not visible over the limited range of velocities in figure 10 and it is immaterial for the subsequent discussion.

Having a robust determination of the speed between the injector and MW02, allows a good prediction of the pellet arrival time in MW05. This in turn gives us the speed between MW02 and MW05 allowing us to predict the arrival time in the monitor. Figure 11 shows the distribution function of pellet arrival times versus predicted arrival times for MW05

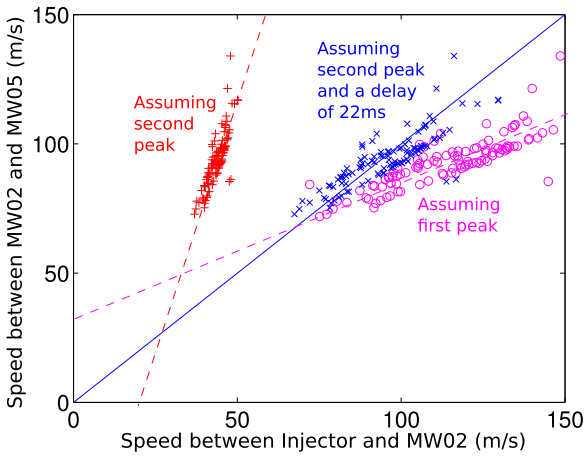

Figure 10. Speed between 1st and 2nd microwave detector as a function of the speed between the injector and the first microwave detector as determined based on the first peak in figure 8 (magenta o), based on the second peak (red +) and based on the second peak with a delay of 22 ms between pellet request and actual launch (blue x).

and for the monitor. All the minor peaks in the distribution functions have now disappeared leaving a single clear peak. This leads to a much more robust identification of individual pellets as they fly through the flight lines allowing their speeds to be determined with confidence.

As mentioned above, an additional microwave cavity, MW03, is situated 0.48 m after MW02. While this detector could not see the pacing pellets before their size was increased in 2017, it now sees most pacing pellets. Given the proximity of MW02 and MW03, identification of pellets between these two signals is straight forward, giving a clear velocity determination to allow a good prediction of the arrival of a pellet in MW05. Since 2017 this measurement has been included to give a more robust identification of pellets and their velocity as they are observed in MW05.

Figure 12 shows the identification of pellets through the flight line for one pulse. The *y*-axis gives the distance from the injector, with a negative offset being applied to the 'request' signal to compensate for the delay between request and launch. This figure shows how a clear tracing of individual pellets through the flight line is achieved. Furthermore, it allows an identification of where individual pellets are lost along the way. Finally, it shows how the variation in speed together with the loss of a number of the pellets along the way, leads to pellets arriving at very irregular intervals in the plasma.

As mentioned at the end of section 2, some pellets arrive in the plasma without being seen by the pellet monitor. We can repeat the analysis from section 2 but basing it on predicted pellet arrival times at the monitor, rather than measured arrival times. Figure 13 shows the probability of an ELM being a triggered ELM as a function of the difference between the ELM time and the predicted triggering time based on the pellet speed in MW05 and disregarding the observation in the monitor. This is overlaid on the probability function from figure 7 based on observations from the pellet monitor. The latter curve is shifted left by 1.95 ms compared to the curve in figure 7, as the *x*-axis in figure 13 is the ELM time relative to the predicted time, while figure 7 showed the ELM time relative to the time the pellet was observed in the monitor. For some ELMs, which, using only the monitor signal, are considered to be highly unlikely to be triggered, this signal can indicate that they are in fact quite likely to be triggered. For investigations, where we are looking to compare the properties of triggered and non-triggered ELMs, this allows us to find such ELMs with confidence. Note that the confidence with which we can say that an ELM is triggered is much lower if this assertion is solely based on the observation in MW05 and hence having a monitor near the plasma is essential to gain any good insight into pellet ELM triggering statistics.

Figures 14 and 15 show overviews of the pellet tracing, pellet speed and ELM triggering information for two pulses as determined through the above analysis. In the pulse shown in figure 14 the pellets were injected from the LFS while the discharge in figure 15 used large pacing pellets and VHFS injection. A number of differences can be seen between these two discharges, perhaps the most notable being the fact that ELMs seem to be triggered much more reliably with VHFS injection. The pellet survival rate also seems to be higher for the larger pellets injected via the VHFS line. Finally, the nature of the ELMs is different in the two discharges, with the second discharge showing bursts of ELMs. This behaviour may be associated with the larger pellet size, the different injection location and perhaps with the fact that these larger pellets have a tendency to break as illustrated in the inset in figure 15.

To get a more quantitative confirmation of the improvement of both pellet survival and ELM triggering probability with the upgrades in 2015 and 2017, a statistical analysis of all the 26 425 pellets mentioned in the introduction has been carried out.

Figure 16 shows the result of this analysis. The data was separated into the following three sets: (i) small pacing pellets, LFS injection prior to 2015; (ii) small pacing pellets, VHFS injection 2015–2017 and (iii) large pacing pellets, VHFS injection since 2017. The left box in figure 16 shows the fraction of the requested pellets arriving at the various detectors along the flight line. Only pellets that are traced through to the location in question are counted. The first column for each of the cases (dark blue) represent the requested pellets and this always takes the value 1 as the histogram is normalised to this number for each set of data. The second column shows the number of pellets arriving in MW02 for the small pellets in (i) and (ii) and the number of pellets arriving in MW03 for the larger pellets in (iii). The third column shows these values for MW04 (LFS injection) and MW05 (VHFS injection). The fourth column shows the pellets seen by the monitor while the final column shows the pellets which trigger ELMs. Some of the larger pellets split before arriving at MW05 and this results in the number of pellets seen here being slightly larger than the ones seen in MW03. This figure clearly shows how the pellet survival was improved significantly by the two upgrades with the fraction of pellets detected in the plasma increasing as follows (i) ∼35%, (ii) ∼53% and (iii) 82%. The overall ELM triggering statistics for the three cases is shown in the

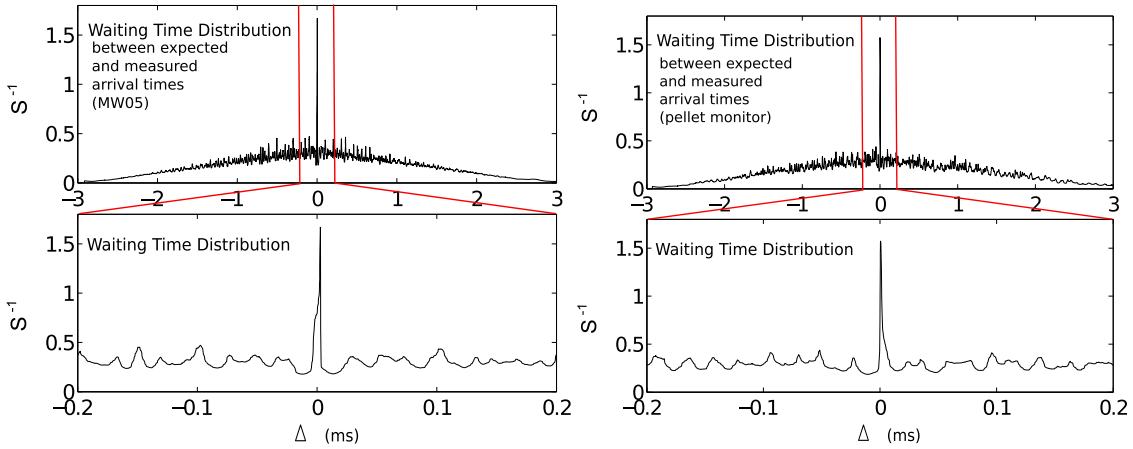

Figure 11. As figure 9, but showing the distribution of the difference between expected and actual pellet arrival times for MW05 (left) and for the pellet monitor (right).

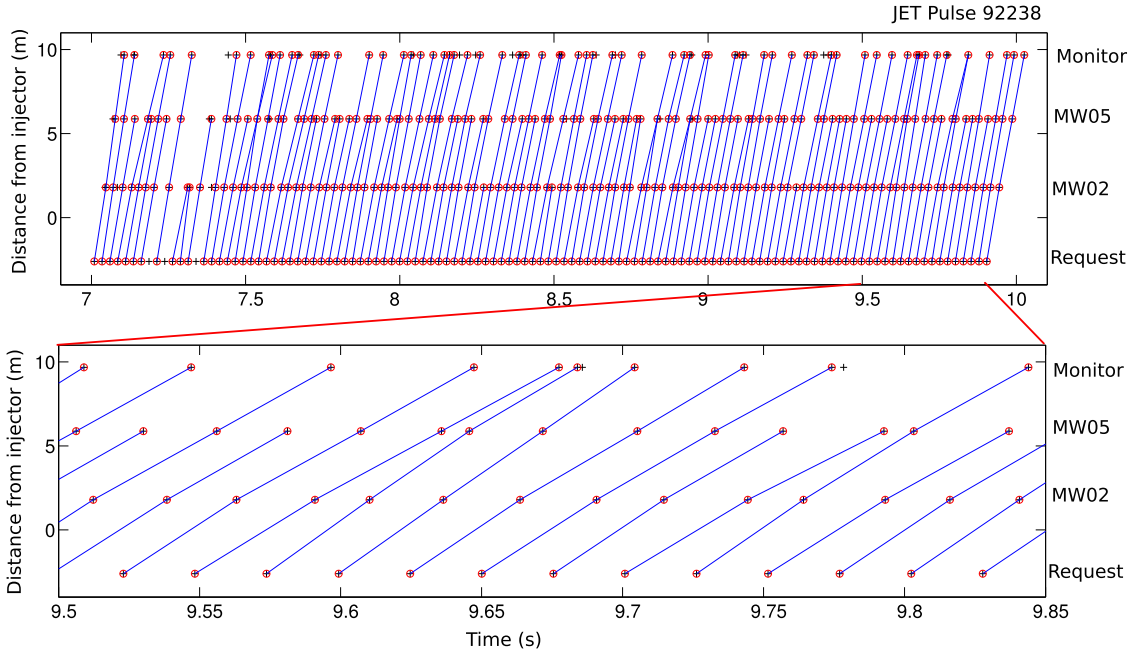

Figure 12. Tracing of pellets through the flight line. The *y* axis shows the location of the various detectors along the flight line. Black + represent a pellet being detected at this location. Red circles around the + indicates that this pellet has been identified with a pellet observed in the previous detector and a blue line shows this link. The slopes of the blue lines represent the pellet speed. The bottom graph shows a zoom over the 9.5–9.85 s range.

right box in figure 16. Here all pellets observed by the pellet monitor are included. For each case, the first column shows the fraction of requested pellets that result in a triggered ELM (orange) and the number that do not (blue). For each case, the second column shows the number of triggered ELMs (orange) and the number of non-triggered ELMs (grey). The ELM numbers are normalised to the number of requested pellets. From this figure it is clear that, even for the smaller pellets, a significantly larger triggering probability is achieved with VHFS launch than with LFS launch. Though a higher fraction of the larger pellets triggers ELMs, the fraction of ELMs that are actually triggered does not increase, showing that there are, on average, more ELMs per pellet after the increase of the pellet size. This is probably linked to the tendency of these larger pellets to create the bursting type of ELMs seen in figure 15.

The observed variation in pellet survival between LFS and VHFS injection, for the same nominal pellet size, is clearly determined by the flight line geometry, while the observed variation in triggering probability is likely to be dominated by differences in the physics of pellet ELM triggering between LFS and VHFS injection.

As can be seen above, there is a large scatter in pellet speed as the pellets arrive in the plasma. The same is true for the pellet size. Though this scatter is not desirable, it forms a good basis for the statistical analysis of the influence of such parameters on the pellets ability to trigger ELMs. Figure 17 shows a scatter plot of pellet speed versus pellet

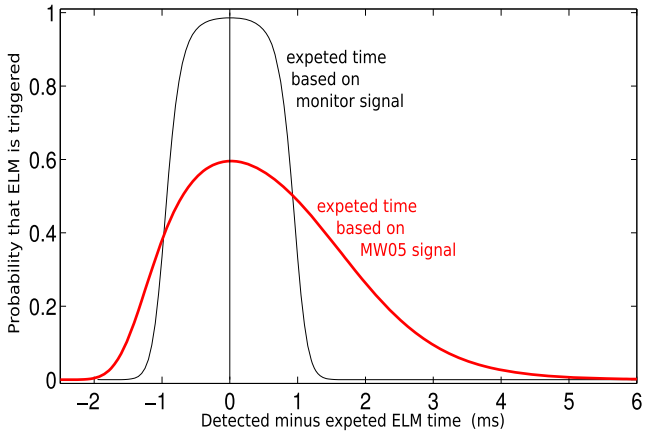

Figure 13. Probability of an ELM being triggered when it is observed a certain time before or after the predicted time. The predicted time based on the pellet speed observed in MW05 is shown in red, while the predicted time based on the observation of the pellet in the monitor is shown in black. The latter curve is a copy of the curve from figure 7 shifted left by 1.95 ms.

size. The red points represent the LFS pellets, the green points represent the smaller (pre-2017) VHFS pellets and the blue points represent the larger (post 2017) VHFS pellets. The size used in this plot is the size determined by MW04 for LFS injection and by MW05 for VHFS injection. Note that the size is given in terms of *electrons*, with 1 mg $= 3.0 \times 10^{20}$ *electrons*. This measure is appropriate as it is the relevant measure for considering the influence on the plasma electron density. The plot clearly shows the higher sensitivity of MW04 than of MW05. This difference has to be taken into account in any statistical analysis. Pellets with sizes too small to be detected by MW05 will clearly have been injected from the VHFS side, especially before the increase of the pacing pellet size. Such pellets may still have been seen by the monitor which detects the pellets as they enter into the plasma but, as no velocity can be ascribed to them, they are ignored in the subsequent analysis.

6. ELM triggering, parametric dependence

In this section we look at the probability of a pellet triggering an ELM as a function of the main pellet parameters: pellet injection location, pellet size and pellet speed. For a specific parameter X (size, speed etc.) we proceed by ordering all the pellets according to the value of X, giving rise to the following sequence:

$$S_X = \left[X_1\ X_2 \ldots X_p \ldots X_h\right], \tag{17}$$

where $X_1 \leqslant X_2 \ldots \leqslant X_p \leqslant \ldots \leqslant x_h$ and h is the total number of pellets included in this analysis. To each pellet we have, in section two, determined a probability T_p that this pellet actually triggered an ELM giving rise to the following sequence:

$$S_{\mathrm{T}} = \left[T_1\ T_2 \ldots T_p \ldots T_h\right]. \tag{18}$$

From these two sequences we can find the following cumulative distributions:

$$C\left(X_p\right) = \frac{p}{h} \tag{19}$$

$$C_{\mathrm{T}}\left(X_p\right) = \frac{\sum_{l=1}^{p} T_l}{h}. \tag{20}$$

Taking the derivative of these cumulative distributions with respect to X, now gives us the distributions $D(X) = C'(X)$ and $D_{\mathrm{T}}(X) = C_{\mathrm{T}}{}'(X)$. From these we can get the statistically determined triggering probability:

$$P\left(\mathrm{Trg}|X = X^*\right) = \frac{D_{\mathrm{T}}(X^*)}{\mathrm{D}(X^*)}. \tag{21}$$

Here $P\left(\mathrm{Trg}|X = X^*\right)$ is the probability of a pellet triggering an ELM under the condition that the parameter X takes the value X^*. In order for the derivatives to be sensible, smoothing needs to be applied to C and C_{T}. Given that we are dividing by D in (21) it is important that D is not too small, which is hard to assure with a simple smoothing function. For this reason, a slightly different approach has been chosen in which we set

$$D^D(X) = \frac{C(X_{n\cdot k}) - C\left(X_{(n-1)\cdot k}\right)}{X_{n\cdot k} - X_{(n-1)\cdot k}} = \frac{k/h}{X_{n\cdot k} - X_{(n-1)\cdot k}}$$

$$\text{For} \quad X_{(n-1)\cdot} < X \leqslant X_{n\cdot k} \tag{22}$$

$$D^D{}_{\mathrm{T}}(X) = \frac{\left(C_{\mathrm{T}}(X_{n\cdot k}) - C_{\mathrm{T}}\left(X_{(n-1)\cdot k}\right)\right)/h}{X_{n\cdot k} - X_{(n-1)\cdot k}}.$$

$$\text{For} \quad X_{(n-1)\cdot k} < X \leqslant X_{n\cdot k} \tag{23}$$

Here k is a fixed integer (the 'bucket' size) and n (the 'bucket' number) goes from 1 to $n_{\max}$ where $n_{\max}$ is the smallest integer for which $k \cdot n_{\max} > h$. Here we take $X_0 = X_1$ and, for $j > h$ we set $X_j = X_h$. $D^D(X)$ and $D^D{}_{\mathrm{T}}(X)$ are discretised approximations of $D(X)$ and $D_{\mathrm{T}}(X)$. This allows us to give the following statistical estimate of the triggering probability as a function of X:

$$P\left(\mathrm{trg}|X \in \left]X_{(n-1)\cdot k}, X_{n\cdot k}\right]\right) = \frac{C_{\mathrm{T}}(X_{n\cdot k}) - C_{\mathrm{T}}\left(X_{(n-1)\cdot k}\right)}{k}. \tag{24}$$

For simplicity we denote $P\left(\mathrm{trg}|X \in \left]X_{(n-1)\cdot k}, X_{n\cdot k}\right]\right) = P\left(\mathrm{trg}|Xn\right)$. The larger the k we chose the lower the 'noise' on this statistically determined distribution but the lower the resolution. To analyse the confidence of the triggering probabilities found in this way, each 'bucket' is considered as a binomial distribution with k elements. 95% confidence intervals are traditionally allocated by assuring that there is a 2.5% chance that the actual value is below the confidence interval and a 2.5% chance that it is above this interval. These intervals are not necessarily symmetric around $P\left(\mathrm{trg}|Xn\right)$ and hence the upper and lower boundaries (p_{un} and p_{ln} respectively) have to be found independently. This can be done either through the exact expressions for the upper and lower confidence boundaries or by more approximate expressions.

The exact values of p_{un} and p_{ln} can be found by solving the following equations [31]:

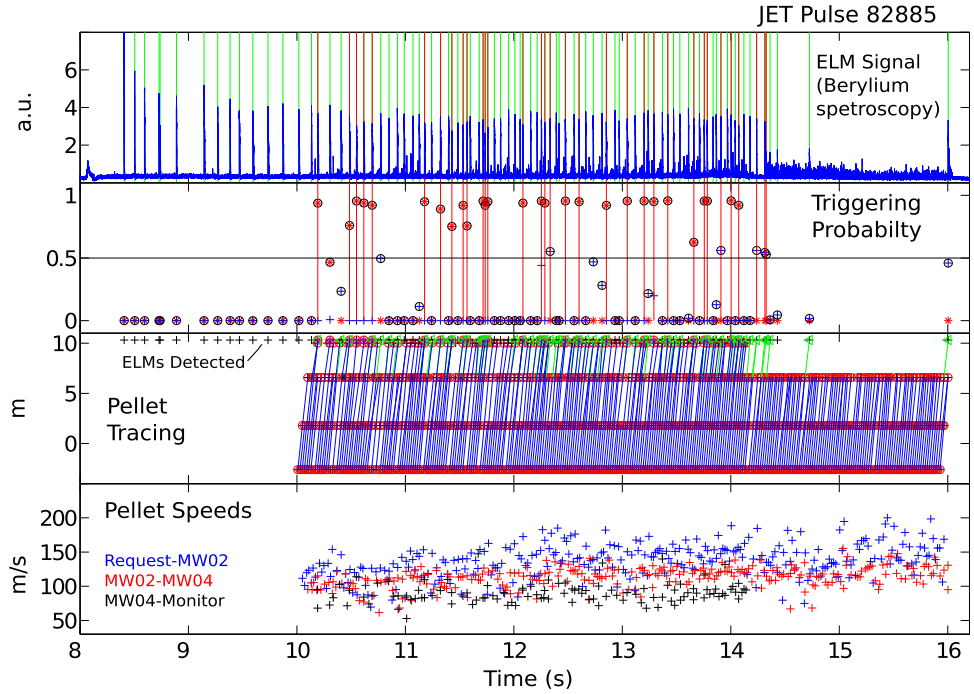

Figure 14. Pulse with LFS pellet injection. (Top box) ELM signal (beryllium spectroscopy) with non-triggered ELMs highlighted by vertical green lines and triggered ELMs highlighted by vertical red lines. (Second box) Probability that an ELM is triggered. Red lines indicate ELMs with triggering probabilities above 50%. (Third box) Pellets traced as in figure 10, green lines indicate probable ELM triggering for pellets not seen in the monitor. (Bottom box) pellet speeds. Note that the monitor signal was not available after 14.1 s.

$$\sum_{m=0}^{N_{Pn}} \binom{k_n}{m} {p_{un}}^m (1-p_{un})^{(k_n-m)} = 0.025 \tag{25}$$

$$\sum_{m=0}^{N_{Pn}-1} \binom{k_n}{m} {p_{ln}}^m (1-p_{ln})^{(k_n-m)} = 0.975. \tag{26}$$

Here N_{Pn} is the nearest integer larger than $P\left(\mathrm{trg}|Xn\right)\cdot k_n$, where k_n is the bucket size for the nth bucket: $k_n = k$ for $n < n_{\max}$ and $k_n = h-(n-1)\cdot k$ for $n = n_{\max}$. The need to find the nearest larger integer here, is due to the use of the values T_p in equation (18) which do not take on only values of 1 or 0, and hence do not give rise to a true binomial distribution of the observations. The actual triggering is, however, a true binomial distribution as a pellet either triggers an ELM or not. Solving the above equations is very computationally intensive for large values of the bucket size. For bucket sizes above ~100 the two-sided Wilson method is much more efficient and it gives very good approximations [31]:

$$p_{un} \cong \frac{P\left(\mathrm{trg}|Xn\right) + \frac{\left(z_{\propto/2}\right)^2}{2k_n} + \sqrt{\frac{P(\mathrm{trg}|Xn)\left(1-P(\mathrm{trg}|Xn)\right)}{k_n} + \frac{\left(z_{\propto/2}\right)^2}{4{k_n}^2}}}{1+\frac{\left(z_{\propto/2}\right)^2}{k_n}} \tag{27}$$

$$p_{ln} \cong \frac{P\left(\mathrm{trg}|Xn\right) + \frac{\left(z_{\propto/2}\right)^2}{2k_n} - \sqrt{\frac{P(\mathrm{trg}|Xn)\left(1-P(\mathrm{trg}|Xn)\right)}{k_n} + \frac{\left(z_{\propto/2}\right)^2}{4{k_n}^2}}}{1+\frac{\left(z_{\propto/2}\right)^2}{k_n}}. \tag{28}$$

Here $z_{\propto/2}$ is the $1-\propto/2$ quantile of the normal distribution. For the 95% confidence interval considered here $z_{\propto/2} = z_{0.025} = 1.96$. In the results presented in the following, the bucket size has generally been kept above 100, thus allowing the use of the much faster equations (27) and (28). For bucket sizes much below 100, the 95% confidence intervals are very large thereby significantly reducing the value of the result in any case.

In the following analysis, the dataset is divided into cases with LFS and VHFS injection. As a starting point all pellets from each of these two separate datasets are considered in the analysis of each parameter. Using such a large database allows the probabilities to be determined with narrow confidence intervals. As can be seen from figure 17, pellet speed and size does not seem to be correlated, thereby rendering this approach valid. There is, however, a difference in the size ranges of pellets used in LFS and VHFS injection experiments. To assess whether this has an impact on the understanding of the influence of parameters other than the size, the analysis was repeated for a reduced dataset, including only pellets with sizes between 1.2×10^{20} and 2.8×10^{20} *electrons*. Another significant difference between the discharges with LFS pellet injection and those with VHFS injection is that virtually all the discharges with LFS injection were carried out with the plasma strike-point located far from the JET divertor cryopump, while the vast majority of the discharges with VHFS injection were carried out with the strike point near the cryopump (see figure 18). As the proximity of the strike-point to the cryopump is known to strongly affect the ELM frequency, this difference could affect the comparison between

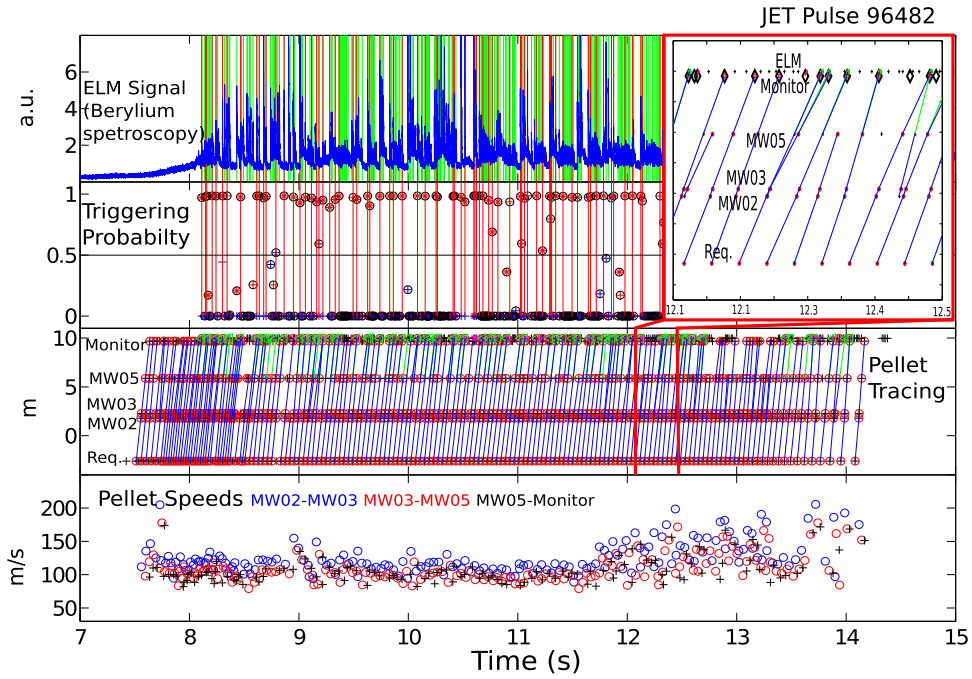

Figure 15. As figure 14, but for a pulse with VHFS injection using the large pacing pellets. The inset shows a zoom of the pellet tracing indicating how pellets sometimes break up in the flight resulting in more pellets (fragments) arriving in the plasma than the number of launched pellets.

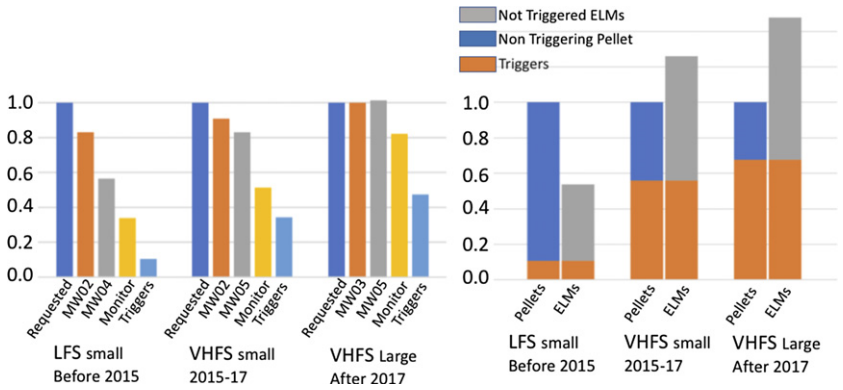

Figure 16. Pellet survival and ELM triggering statistics for the three configurations. (Left) Pellet survival through the flight line. (Right) ELM triggering statistics.

the triggering probabilities. Fortunately, a limited set of discharges with VHFS pellet injection used a strike point position far from the cryopump. Though resulting in an analysis with large error bars, repeating the analysis for this limited dataset allows the assessment of whether the difference in strike-point location has a strong impact on the comparisons between ELM triggering probabilities with LFS and VHFS pellet injection.

One of the interesting observations which led to the decision to move the pellet injector to achieve reliable VHFS launch was the impression that pellets could trigger ELMs very soon following a previous ELM with VHFS launch, while it was very difficult to trigger ELMs much earlier than 20 ms after the previous ELM when using LFS launch [25, 30]. The ability to trigger an ELM soon after a previous ELM is likely to be very important for ITER as the required increase in ELM frequency could be up to a factor of 10 in order to reduce the ELM load sufficiently [12]. As described in the introduction this impression was based on very limited data and it is therefore interesting to see if this observation can be confirmed now that we have a large number of discharges with VHFS launch. Figure 19 shows the probability of a pellet triggering an ELM as a function of the difference Δt between the pellet arrival time and the time of the last ELM prior to the pellet in question: $P\left(\mathrm{trg}|\Delta t\right) \equiv P\left(\mathrm{trg}|\Delta t = \Delta t^{*}\right)$. The probability is given separately for LFS and VHFS pellet launch. In interpreting this figure, note that the ELM detection algorithm used to find the ELM times only detects ELMs which occur more than 5 ms after a previous ELM. Thus, an ELM triggered by a pellet arriving before ~4 ms after the previous ELM would not be detected and the pellet would not be seen as 'triggering'. For this reason, only pellets arriving at least 5 ms after the

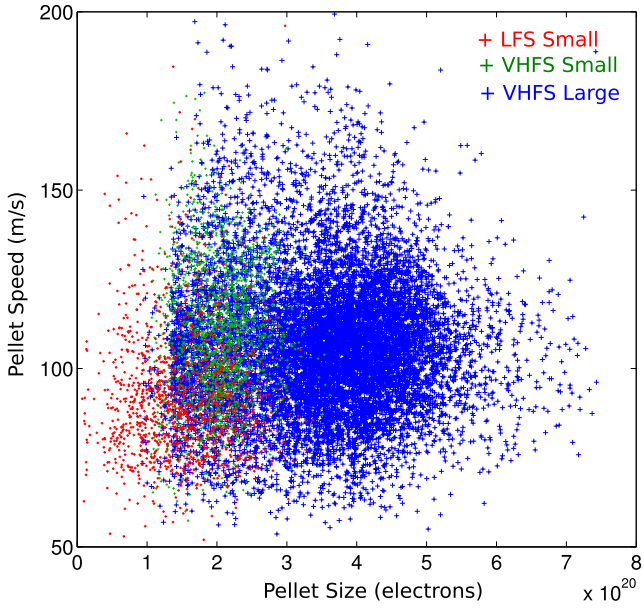

Figure 17. Distribution of pellet speed and size for all pellets used in the analysis.

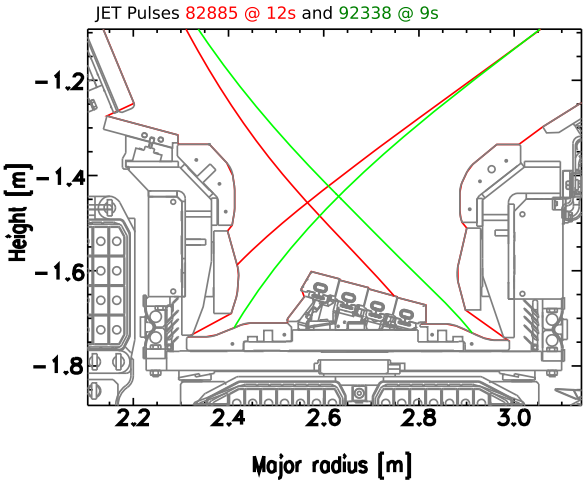

Figure 18. Typical divertor configurations used before 2015 (red) and after 2015 (green) The JET cryopump is situated near the bottom right corner of the image (not shown).

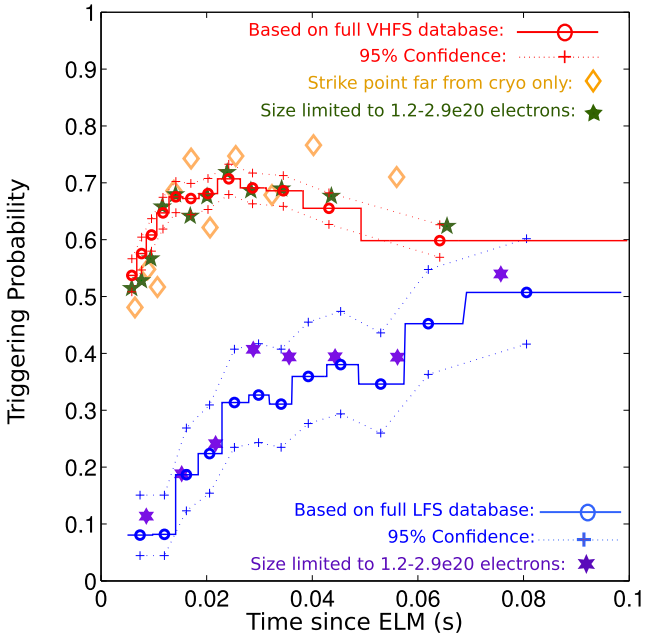

Figure 19. Triggering probability as a function of pellet arrival time relative to the previous ELM, for LFS and VHFS pellet injection. See text for details.

previous ELM are included in the current analysis. The choice of a minimum of 5 ms between detected ELMs has been made to avoid secondary ELMs in the tail of a larger ELM being detected as separate ELMs. In figure 19, the full lines represent the triggering probabilities determined from the full database. The horizontal extent of each step in these lines represent the range covered by each of the 'buckets' used in the analysis. As each bucket contain the same number of pellets, the horizontal extent of these lines represents the inverse of the 'density' of pellet arrival times. Small circles sitting on the horizontal lines represent the 'centre of gravity' of the arrival times of the pellets for each bucket. The crosses linked by dotted lines show the confidence intervals calculated as described above. A few additional points are included in this figure to evaluate whether the differences between the experiments with LFS and VHFS pellet injection, described above, have a significant influence on the observed triggering probabilities. The purple and green stars represent the values found by restricting the included pellet sizes to the range $\left[1.2 \times 10^{20}, 2.8 \times 10^{20}\right]$ *electrons* as described above. Similarly, the orange diamonds represent the values found for VHFS pellet injection when restricting the database to discharges with the strike point far from the cryopump. The wider confidence ranges associated with the reduced databases are not shown in figure 18, in order not to clutter this figure too much. The larger scatter resulting from the reduced datasets is however evident, especially for the data from VHFS pellet injection into plasmas with the strike point far from the cryopump. The most important observation is, however, the fact that there is no indication that restricting the database changes the result. Similar tests have been performed for the analyses of the influence of pellet size and pellet speed on ELM triggering probability. Again, the restriction of the database did not result in any change in the conclusion and hence the points associated with the analysis based on reduced databases are not included in the figures showing these analyses.

The most eye-catching feature of figure 19 is the fact that VHFS launch leads to a much higher triggering probability than LFS launch. The second clear observation is that, while the triggering probability increases slowly with Δt for LFS launch, starting near 0% and reaching about 50% for Δt >70 ms, a large triggering probability >50% is seen even at the lowest Δt values of 5 ms followed by a modest increase up to 70% triggering probability for Δt >15 ms, for VHFS injection. The reason for the slight decline for larger values of Δt for VHFS injection is not obvious, though most plasmas included in the analysis have natural ELM periods <40 ms and hence the points associated with larger values of Δt are likely

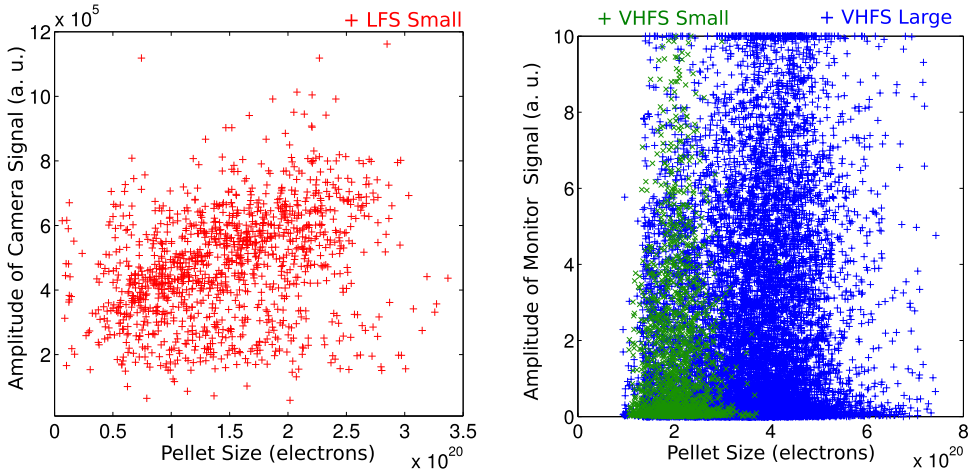

Figure 20. Amplitude of camera/monitor signal as a function of pellet size measured in the last MW cavity in the flight lines for all pellets included in this analysis. (Left plot) LFS injection—pellets seen by the camera, (right plot) VHFS injection—pellets seen in the monitor. Green points represent the small pellets injected before 2017 while blue points represent the larger pellets injected after 2017.

to come from plasmas in which ELM triggering is particularly difficult for a range of reasons, which it is beyond the scope of this paper to discuss. Note that, rather than finding the triggering probability as a function of the time since the last ELM, what we would really like to determine is how early, compared to the next natural ELM we can trigger an ELM. This is, however, very hard to ascertain. We cannot get the natural ELM frequency based on a discharge without pellets, as the pellets themselves fuel the plasma and they therefore are likely to change the underlying ELM frequency in a way that is hard to determine.

The main observation to take away from the current analysis, is that we can confirm that triggering, in particular soon after a previous ELM, is indeed significantly easier with pellets launched from the VHFS than for pellets launched from the LFS, confirming that the decision to move the pellet injector to its high position, was indeed justified.

The main other properties of the pellets which one would expect would influence the ability of pellets to trigger ELMs is the pellet size and the pellet speed [16, 21]. Analysing the influence of the pellet size is not straight forward. For the pellet monitor used to detect pellets arriving from the VHFS line, the amplitude of the signal does not give much information about the size of the pellet. In fact, as mentioned in section 2, some pellets are not seen at all in this monitor. It is clear that a large signal in the monitor does represent a large pellet, but the converse is not true. For the monitor used to detect pellets from the LFS line, the situation is better, with all pellets of a decent size being detected and with the amplitude of the signal being correlated, though not linearly, with the pellet size. Better information about pellet sizes can be had from the microwave cavities situated where the pellets enter into the vacuum vessel. These give a good quantitative measurement of the size of the pellets, though the cavities at the entrance to the vacuum vessel are not identical for the LFS and VHFS lines, with the VHFS cavity being less sensitive and hence measuring only slightly larger pellets. Figure 20 shows the amplitude of the monitor signals near the plasma as a function of the pellet size seen in the microwave cavities just outside the vacuum vessel. The left plot shows the data for LFS injection while the right plot shows VHFS data. In the latter, the green points are for the nominally smaller VHFS pellets injected before 2017 while the blue points are for the larger pellets injected after 2017. This figure illustrates a number of issues affecting the attempt to study the influence of pellet size on ELM triggering ability.

- For the LFS data there is a correlation between the amplitude of the monitor signal and the pellet size determined by the microwave cavity, but there is clearly a large scatter. This scatter is probably mainly due to pellets being damaged/eroded as they fly through the final part of the flight line. Some of the outliers may also be associated with miss-identification of pellets.
- Again, for the LFS, the best trend line does not go through 0. This indicates that the monitor signals are not linear with pellet size.
- For the VHFS data, there is hardly any correlation between monitor amplitude and pellet size measured by the microwave cavity, though the larger pellets injected after 2017 give rise to large monitor signals more frequently. The main observation is, however, that the bulk of the pellets seen in the monitor show a much lower amplitude, regardless of their size as seen in the microwave cavity.
- The lowest level for detecting pellets in the microwave cavity is significantly larger for the VHFS cavity than for the LFS cavity. This in turn means that it is likely that a significant number of pellets arrive in the plasma without being seen in the microwave cavity on their way.

Figure 21 (left) and (right) shows ELM triggering probabilities as a function of the pellet monitor and microwave cavity signal amplitudes respectively: $P\left(\mathrm{trg}|Mn\right) \equiv P\left(\mathrm{trg}|\mathrm{mon} = Mn\right)$ and $P\left(\mathrm{trg}|Sz\right) \equiv P\left(\mathrm{trg}|\mathrm{MWSize} = Sz\right)$.

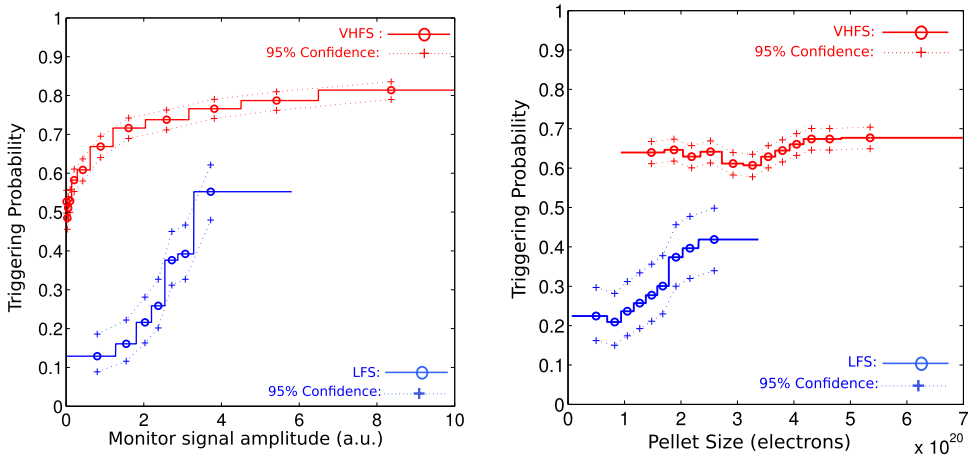

Figure 21. ELM triggering probabilities as a function of the signal amplitudes of the signals observing the pellets; (left plot) as they arrive at the plasma (monitor/camera signals) and (right plot) just before they enter into the vacuum (microwave cavity signals). For the microwave signals an attempt has been made to achieve an absolute calibration of the pellet size in 'electrons'. The two microwave cavities are different and hence the absolute calibrations could suffer from different systematic errors. The two monitor signals are even more different as described in the text.

As already described above the amplitude of the monitor signal for the VHFS signal does not represent the pellet size well. This is clearly seen from figure 21 (left), where even pellets giving rise to a minuscule monitor signal triggers ELMs with rather high probabilities. Thus, even small monitor signals may represent decent sized pellets. Large monitor signals, on the other hand, clearly represent large pellets. For such large pellets the figure shows a triggering probability of 80%–85%.

For the LFS monitor the correlation between the monitor signal amplitude and the pellet size is much better and here we see a clear increase in the triggering probability with increasing monitor signal amplitude as already reported in [25], with the triggering probability approaching the average VHFS triggering probability for the largest LFS pellet sizes.

To try to get a better handle on the influence of the pellet size on the triggering probability both for VHFS and LFS launch, we have to turn to the microwave cavity signals. For these signals we have a reasonable absolute calibration. Figure 21 (right) confirms that the triggering probability increases significantly with the pellet size for LFS launch even when using the signal from the last microwave cavity to determine the pellet size. This increase is less clear than the one seen based on the monitor signals used in figure 21 (right), due to the variation in the pellet degradation in the flight line between the microwave cavity and the monitor.

For the VHFS pellets, the dependence of triggering probability on the size of the pellet as seen in the final microwave cavity is not at all clear. Figure 21 (left) would indicate that a dependence on size exists, but this dependence is weak enough that the size seen in MW05 does not show a statistically clear influence on the triggering probability. More importantly, good triggering probability ∼65% is achieved even for the smallest pellets seen by the VHFS MW cavity. This seems to indicate that the overall dependence on pellet size is much less significant for VHFS injection than for LFS injection, though

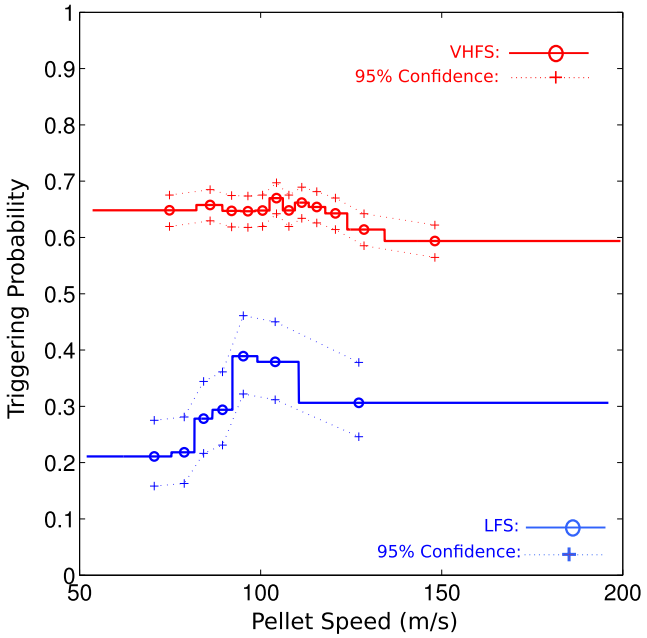

Figure 22. Speed dependence.

there could be a sharp drop in triggering probability for pellets smaller than the lowest size detectable by the VHFS monitor ($\sim 1.0 \times 10^{20}$ electrons).

Turning to the pellet speed, the analysis is less complicated as we have established a robust pellet speed determination based on the flight time between the last MW cavity and the pellet monitor as described in section 3. For LFS launch [25] reported that the ELM triggering probability increased strongly with pellet speed. Figure 22 shows the triggering probability as a function of pellet speed $P\left(\mathrm{trg}|Sp\right) \equiv P\left(\mathrm{trg}|\mathrm{Speed} = Sp\right)$ for both LFS and VHFS launch. The LFS database used in [25] has been extended and this now includes some pellets with higher velocities. This extension seems to indicate that, for LFS launch, there is a maximum speed

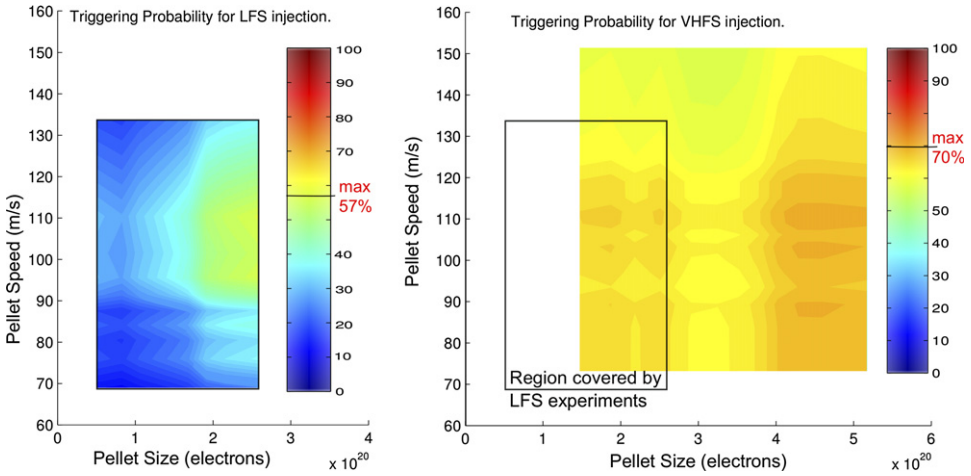

Figure 23. Combined speed and size: (left plot) LFS injection (right plot) VHFS.

beyond which the triggering probability seems to decrease again. As can be seen by the confidence intervals shown in figure 22 this decrease may not be significant, though it could be worth investigating whether such a maximum can be expected theoretically. For VHFS launch the main observation is, other than the much higher average triggering probability, the almost complete independence of the triggering probability on the pellet speed. A slight, possibly not significant, decrease in triggering probability is seen for faster pellets. It is however interesting that this decrease is observed for both LFS and VHFS launch, while the increase with speed for lower velocities is only seen for LFS launch.

The dependence of the ELM triggering probability on the combined pellet speed and size can be found from the following simple equation

$$P\left(\mathrm{trg}|\mathrm{Size} = Sz \wedge \mathrm{Speed} = Sp\right) = \frac{P\left(\mathrm{trg}|Sz\right) \cdot P\left(\mathrm{trg}|Sp\right)}{P\left(\mathrm{trg}\right)}. \quad (29)$$

This equation holds true if (a) the shape of $P\left(\mathrm{trg}|Sz\right)$, considered as a function of the pellet size, is independent of the pellet speed and (b) the shape of $P\left(\mathrm{trg}|Sp\right)$, considered as a function of pellet speed is independent of the pellet size. To verify the validity of this assumption the whole size—velocity space can be divided into a number of regions ('buckets') and the probabilities can then be found separately for each of these regions. This leads to small 'bucket' sizes or very large regions. Having performed this calculation and compared with the findings based on equation (29), no differences outside the error bars were found and hence the use of this equation seems valid.

Figures 23 (left) and (right) shows the combined triggering probability dependence on pellet speed and size as measured by the MW04 and MW05 for LFS and VHFS pellet injection respectively. There is a very marked difference between these two figures. While the maximum triggering probabilities are not hugely different, the triggering probability vary strongly as a function of pellet size and speed for LFS injection, while it hardly varies at all as a function of these quantities for VHFS injection. A black rectangle is added in the right plot in figure 23 showing the area covered by the LFS data. This rectangle shows that, though the ranges covered in the two figures, are not the same, there is a large overlap. This indicates that the difference between the figures is not predominantly due to the different speed and size ranges covered in the two cases. Note that this figure considers the mean probability values from figure 21 (left) and figure 22. The values found this way will be affected by the confidence intervals and hence the triggering probabilities in figure 23, especially for LFS injection will suffer from large error bars. Note also that that pellets arriving down to $\Delta t = 5$ ms after the previous ELM are included in this analysis. This penalises the LFS probability strongly. Including only pellets arriving later would increase the triggering probabilities for LFS injection significantly as discussed below. Though using the mass signals from MW04 and MW05 is the only way to get some quantitative measure of the pellet size this value is likely not to be representative of the actual size of the pellet as it enters into the plasma. The camera signal for the LFS injection, though not giving a value which can be calibrated in mass, gives a clearer picture of the relative sizes of the pellets as illustrated by figure 21 (left). This is to a certain extent true even for the pellet monitor looking at the VHFS injection, in particular for pellets giving rise to large signals in this monitor.

Figure 24 shows the triggering probabilities based on the amplitude of the signals from the camera (LFS) and pellet monitor (VHFS). To reduce the influence of the pellet arrival time with respect to the previous ELM, which has a very strong influence for small values of this time, especially for LFS injection, the database has been restricted to pellets arriving at least 20 ms after the last ELM. Though quantitative information on the pellet size has been lost by using the camera and monitor signals, figure 24 gives a better idea of dependence of the triggering probability on the relative pellet sizes. Figure 24 (left) shows that, for LFS pellets arriving at least 20 ms after the previous ELM, the predicted triggering probability reaches $\sim$100% for the maximum pellet size and the optimal velocity; in agreement with the value given in [25]. This value would be expected to have a large (negative) error bar when considering the confidence intervals shown in figures 21 and 22. As

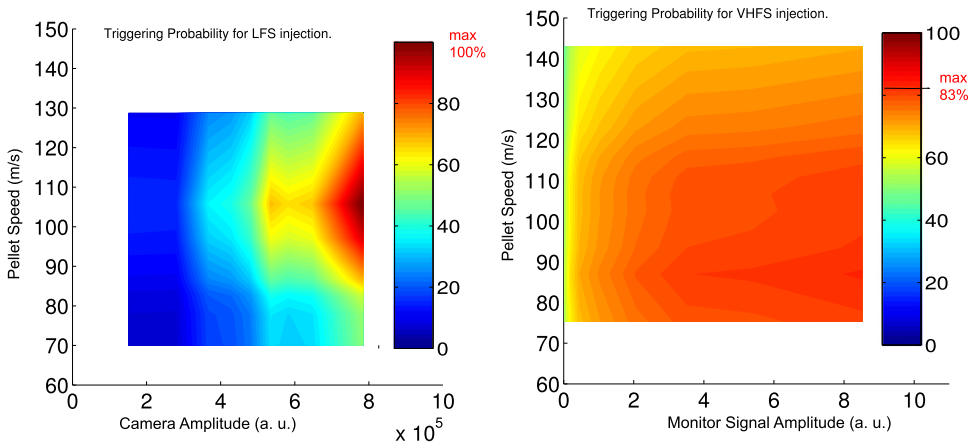

Figure 24. Combined speed and camera/monitor amplitude: (left plot) LFS injection, (right plot) VHFS injection.

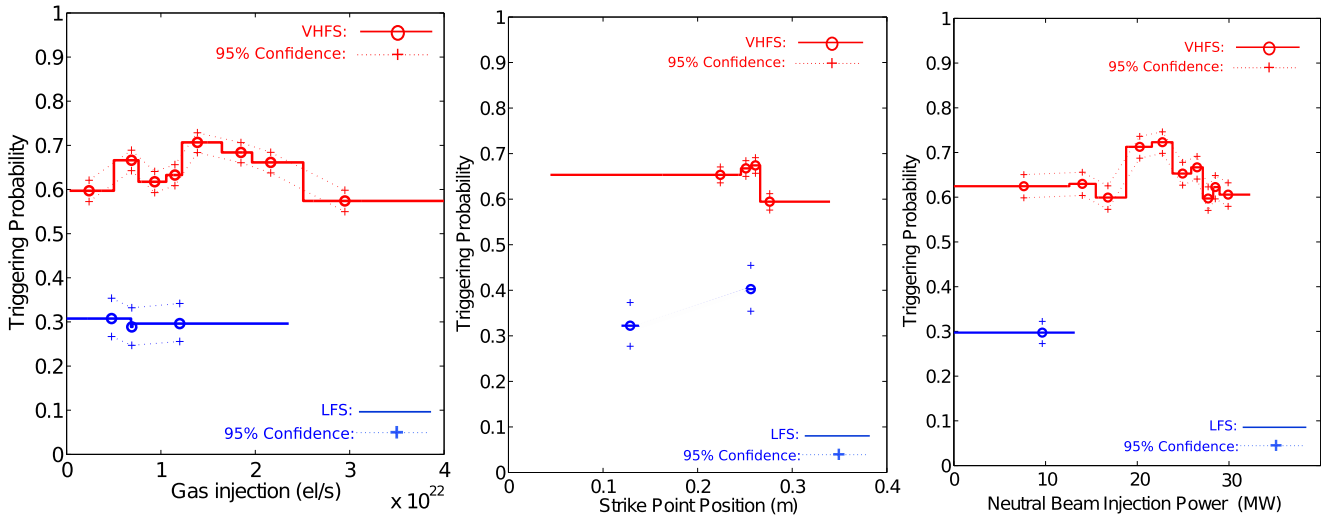

Figure 25. ELM triggering probabilities as a function of the main parameters which are normally seen to affect the ELM frequency: (left) gas injection rate. (Middle) Strike-point position. (Right) Neutral beam power. No clear dependencies on these parameters can be detected within the error bars.

in figure 23, the VHFS plot shows a rather flat landscape, with the maximum triggering probability reaching 83%. The VHFS plot is based on a significantly larger statistics with narrower confidence intervals. Considering the confidence intervals, the difference between the maximum triggering probabilities seen in the LFS and VHFS cases is probably not significant but it is clear that good triggering probabilities for LFS launch can only be achieved at least 20 ms after the previous ELM and with pellet parameters within a very narrow range.

The analysis described above has considered all H-mode discharges with clear distinct ELMs—mainly type 1 with some compound ELMs. For the discharges with VHFS launch, the engineering plasma parameters cover most of the JET operational domain, with the plasma current and the toroidal field spanning 1.5–3.8 MA and 2.0–3.4 T respectively. The NBI power is between 9 MW and 32 MW, with the minimum being determined by the requirement to be in an ELMy H-mode and the gas injection ranges between 0 and $\sim 1 \times 10^{23}$ electrons/s, the range mainly determined by staying with type-1 ELMs. Finally, the strike-point position was varied as described earlier. For the discharges with LFS launch, the range of parameters was much smaller, with plasma currents and toroidal fields limited to a narrow range around 2 MA and 2.3 T respectively. Hence a study of the ELM triggering probability as a function of these parameters can only be carried out for VHFS launch. The method for evaluating the dependence of the triggering probabilities used in the preceding, has been applied to these parameters and the results are shown in figures 25 and 26. The points for LFS are included for comparison in these figures, though the range of parameter variation for LFS launch is very limited.

Figure 25 shows the triggering probabilities as a function of gas fuelling rate, strike point position and NBI injection power. For discharges at the same plasma current and toroidal field, these three parameters have been seen, experimentally, to have the strongest influence on the ELM frequency, in the absence of pellet injection. For this reason, one could expect that the ability of pellets to trigger ELMs may depend on

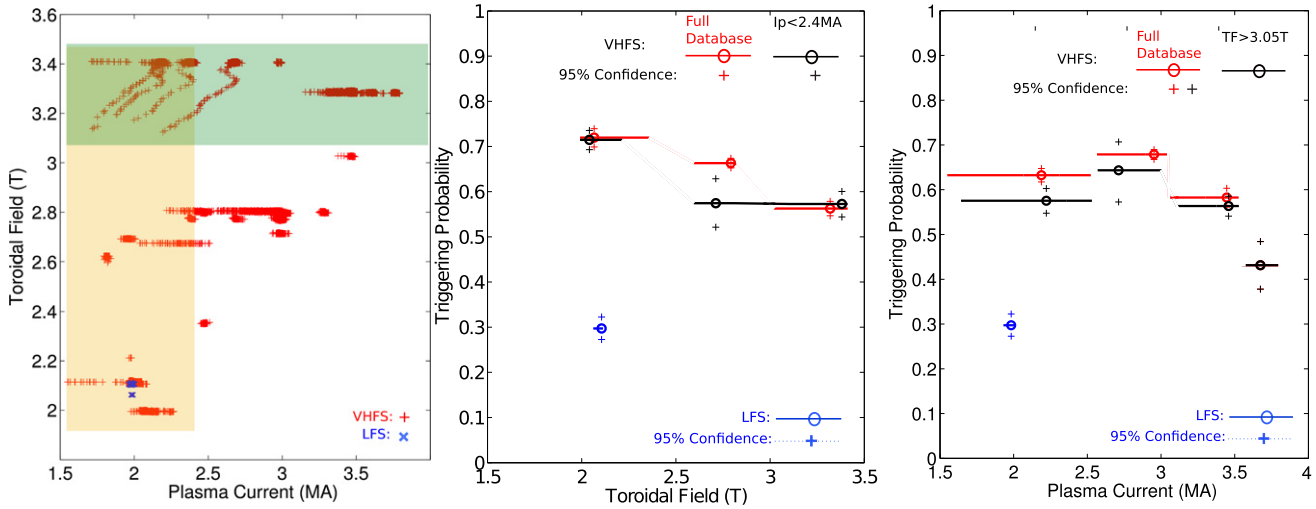

Figure 26. ELM triggering probabilities as a function of toroidal field and plasma current. (Left) The range of variation of plasma current and toroidal field. For LFS plasma injection (blue x) all discharges were around 2 MA and 2.3 T. For VHFS launch there is a co-linearity between toroidal field and current (high current can only be achieved at high toroidal field). (Middle) Triggering probability as a function of toroidal field. Red curve—based on the full database. Black curve based on discharges with plasma current less than 2.4 MA (orange shaded area in the left graph)). (Right) Triggering probability as a function of plasma current. Red curve—based on the full database. Black curve based on discharges with toroidal field larger than 3.1 T (green shaded area in the left graph)).

these parameters, however no clear dependence is seen in figure 25.

Figure 26 shows the dependence of the triggering probability on toroidal field and plasma current. The left graph of figure 26 shows the existence diagram of the combinations of toroidal field and plasma current at the time when pellets are injected. This highlights the co-linearity between these two parameters, with high plasma current only being achievable at high toroidal fields, due to the limitation of the edge safety factor q_{95}, where plasma stability is severely compromised for q_{95} much below 3. The middle and right graphs of figure 26 show the dependences of the triggering probability on toroidal field and plasma current respectively. Here the red traces show the dependences derived from the full database, whereas the black traces show the dependences for reduced databases. For the middle of figure 26, the reduced database considers only points with plasma current below 2.4 MA as shown shaded in orange in the left graph of figure 26. Similarly, for the right graph of figure 26 the reduced database considers only discharges with toroidal field above 3.1 T as show shaded in green in the left graph of figure 26. A weak decrease of the triggering probability with toroidal field is observed and a slightly stronger decrease for increasing plasma current is seen, in particular for the largest plasma currents. These dependences are, however, weak and good triggering probabilities are achieved for all explored toroidal fields and plasma currents. One could speculate that the weak degradation in triggering reliability at higher toroidal fields and plasma currents is likely to be associated with the fact that the additional heating power in such plasmas is not as far above the L-H threshold as would be desirable.

The main message from this investigation is that, while pellet triggering through LFS injection depends strongly on the pellet size and speed, triggering using VHFS injection is very robust and even at low pellet speed, moderate size pellets triggers ELMs with high reliability over the full range of plasma parameters explored in these experiments.

7. Discussion

The most notable observation which can be made from the above analysis, is the very clear increase in ELM triggering probability for pellets launched from the VHFS with respect to pellets with similar properties launched from the LFS. This difference is particularly evident for pellets arriving very soon after an ELM. As a matter of fact, it has been seen to be almost impossible to trigger ELMs with pellets launched from the LFS, if these pellets arrive less than 20 ms after an ELM. On the other hand, pellets launched from the VHFS readily trigger ELMs as soon as 5 ms after the previous ELM, where 5 ms is taken as a minimum ELM interval for the analysis, to avoid detecting secondary ELMs following a large ELM. The fact that ELMs can be triggered so close together is very important for ITER and other future machines, where the ELM period has to be radically reduced with respect to the natural ELM period, in order for the ELM size to be acceptable. This observation is in good agreement with the expectations based on JOREK simulations described in section 2, which indicate that the favourable pellet drift direction will allow even slow and small pellets launched from the HFS side to penetrate far enough into the plasma, to create sufficiently large seed modes and initiate the unstable growth of these modes, even very soon after a previous ELM. The unfavourable drift of pellets launched from the LFS would mean that such pellets would need to be larger and faster in order to achieve the same effect. Another important, and perhaps more surprising, observation is that, for VHFS injection, the ELM triggering probability only depends very weakly on parameters such as pellet size

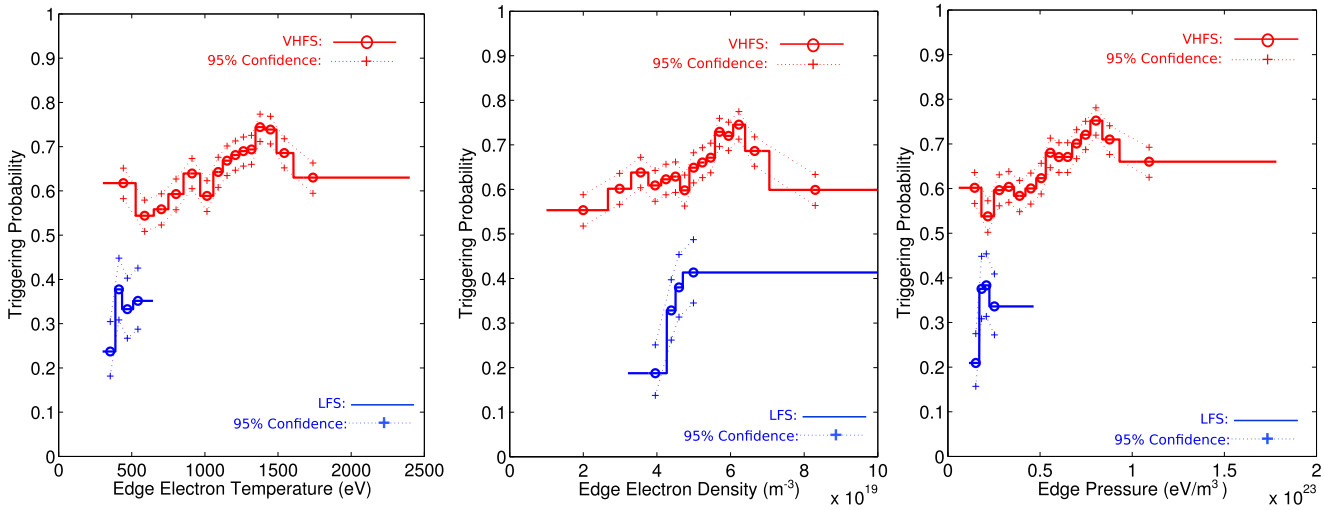

Figure 27. ELM triggering probabilities as a function of the plasma edge (pedestal top) parameters: (left) edge electron temperature. (Middle) Edge electron density. (Right) Edge electron pressure (product of electron temperature and density).

and speed and even on the time elapsed since the last ELM. The fact that triggering, with good reliability, is possible very soon after an ELM with VHFS launch, shows that the pellets, included in this analysis, are large enough to trigger ELMs, even when the unperturbed plasma is far from the stability boundary. This would explain that the triggering probability only depends very weakly on the pellet size and other parameters, since the pellets that we detect are already big enough to trigger ELMs even in rather unfavourable conditions. Another factor which may affect the dependence of triggering probability on the various parameters explored, is the modifications to the underlying plasma caused by injecting strings of pellets. In particular when injecting pellets from the VHFS, these pellets cause substantial fuelling, leading to an increase in the underlying ELM frequencies with the result that the number of natural ELMs increases at the same time as the number of triggered ELMs increases. This would indicate that the plasma moves closer to the stability boundary and hence ELM triggering would be expected to become easier during the injection of strings of pellets.

The situation is clearly very different for LFS launch, where a very strong dependence on the time since last ELM is seen. This indicates that the perturbation introduced by most LFS pellets which reach the plasma soon after an ELM crash are not large enough to induce unstable modes. This means that, for LFS launch, the size of the perturbation induced is marginal with respect of the threshold for inducing unstable modes. As a consequence, the triggering probability depends strongly on other parameters such as pellet size and speed etc. This is readily explained by the natural pellet drift, which tends to expel pellets from the plasma for LFS injection. As a consequence, larger pellet velocities are required to overcome this drift and allow the pellets to penetrate far enough into the plasma.

The engineering parameters which are normally used to modify the natural ELM frequency, do this by modifying the plasma edge parameters. It is therefore of interest to see how these plasma edge parameters affect the reliability with which pellets trigger ELMs. This would help to confirm the assertion that, for VHFS discharges, the pellets are large enough to trigger ELMs over a wide range of edge conditions. Figure 27 shows the triggering probabilities as a function of edge electron temperature, edge electron density and edge electron pressure, where the edge pressure is taken as the edge temperature multiplied by the edge density. The edge density is taken as the line average density measured by a vertical interferometer channel (channel 4 [32]), which passes about 5 cm inside the top of the edge pedestal in the experiments analysed here. The edge electron temperature at the same radial location is measured by the JET electron cyclotron emission diagnostic [33]. The temperature, density and pressure values are taken immediately before a pellet enters the plasma. Figure 27 is derived, based on the entire database used in section 6. For LFS injection, a fairly strong dependence of the triggering probability on these parameters is seen. This is particularly clear for the edge density dependence. This is in good agreement with the low triggering probability observed for LFS injection when pellets arrive in the plasma soon after a previous ELM, when the edge temperature and density has been strongly reduced by the ELM. For VHFS injection, the dependencies are rather weak, despite the range of variations of these parameters being significant. This confirms that the pellets injected from the VHFS side are large enough to trigger ELMs even when the edge pedestal has not grown very large. Looking at figure 27 in more detail, a moderate increase in triggering probability with increasing edge temperature and density is seen up to temperatures of 1.5 keV and densities of 6×10^{19} m^{-3}. This is understandable as an increase in temperature and density corresponds to the plasma state moving closer to the instability boundary, which should render triggering easier. The subsequent decrease in triggering probability for even higher temperatures and densities is less easy to explain, though it corresponds with the similar decrease for pellets arriving more than 30–40 ms after the previous ELM, as seen in figure 19. It is clear that there are significantly fewer instances of temperatures and densities above

1.5 keV and 6×10^{19} m^{-3} respectively. Such high edge temperatures and densities most likely correspond to plasmas which are more peeling–ballooning stable. Investigating the mechanism for this behaviour for the limited number of relevant points in the database, though interesting, is beyond the scope of this article.

The above analysis indicates that ELM triggering with VHFS pellets seems very robust and that it does not depend strongly on any of the parameters investigated in this study as long as the pellets are large enough to be detected by MW05 (mass > 0.5 mg $= 1.5 \times 10^{20}$ electrons). For smaller masses there clearly is a reduction in the ability of pellets to trigger ELMs as seen in figure 21, though the current diagnostics cannot quantify this. For LFS injection the triggering reliability, on the other hand, depends strongly on both pellet properties and underlying plasma parameters. For pellets injected from the LFS, the pellet size needs to be near the maximum available (1.5×10^{20} electrons) and the pellet velocity needs to be at least 100 m s^{-1} in order to achieve high ELM triggering probabilities. Even in this case reliable triggering can only be achieved after at least 20 ms has elapsed since the previous ELM. For DIII-D the required pellet sizes, determined by JOREK, assuming pellet speeds of 100 m s^{-1} are 2.3×10^{20} electrons and 8.6×10^{19} electrons for LFS and HFS launch respectively [21]. The pellet properties required for reliable ELM triggering determined for JET in the current study, both for LFS and VHFS injection, are therefore in good qualitative agreement with these JOREK findings for *D*III-*D* [21]. One would expect to require somewhat larger pellet for JET than for *D*III-*D*, given the different size of the two machines and hence the current investigations indicates that the JOREK simulations are likely to be slightly pessimistic in agreement with the statements in [21]. The current investigations add confidence to JOREK based ITER extrapolations, where the required pellet size assuming X-point pellet injection is estimated as 2.0×10^{21} electrons.

8. Summary and conclusions

The analysis presented above gives a solid base for determining whether a specific pellet triggers a certain ELM. Having a robust determination of this allows a detailed analysis of the properties of pellets which affect their ability to trigger ELMs and the differences between triggered and non-triggered ELMs. While the latter investigation, which is ongoing, is beyond the scope of this paper, the ELM triggering dependence on pellet parameters has been investigated in some detail. The main observation is that the location from which the pellets are injected plays a very significant role, with injection from the HFS (or more specifically the VHFS) resulting in much more reliable ELM triggering than injection from the LFS. Furthermore, the triggering ability seems to depend only very weakly on the pellet characteristics for VHFS injection. It is particular important to note that, though the triggering probability is reduced slightly when a pellet arrives very soon after a previous ELM, this probability still remains high. This is in marked contrast with LFS injection where the triggering probability increases strongly with the time elapsed since the last ELM, pellet size and the pellet speed and where triggering earlier than 10–20 ms after the previous ELM proved virtually impossible. Though not necessarily significant, the results presented hints at the possibility that there is an optimal pellet speed for ELM triggering. This may indicate that pellets which are too fast will go too far into the plasma before ablating, depositing too little mass in the critical part of the plasma edge. It would be interesting to see if simulations with JOREK could confirm this possibility.

In general, it is desirable to reduce the fuelling associated with pellet ELM pacing as much as possible. This would, on its own, seem to lead to the choice of low field injection, as the fuelling efficiency is much lower for the same size pellets. The current investigation shows that this choice may not be optimal, as the lower fuelling efficiency is counteracted by the need for larger and faster pellets to trigger ELMs reliably—which would increase the fuelling. Using the HFS injection, even very small pellets seem to be able to trigger ELMs and the required pellet size in this case is mainly determined by the size required to improve the chance of the pellets surviving the transport through the flight line to the plasma. Hence with a robust transport, it may be possible to use very small pellets, thus reducing the fuelling significantly. A probably more important, argument against using LFS injection, is the difficulty of triggering an ELM soon after the previous ELM. This would lead to a maximum achievably ELM frequency and this maximum may not, in future devices, be high enough to reduce the ELM load sufficiently.

For VHFS injection, only a very weak dependence of the triggering probability on engineering plasma parameters such as plasma current, magnetic field, plasma fuelling rate etc. were found. Further investigations of the dependence of the triggering probability on plasma edge parameters similarly showed a weak dependence on the plasma density and temperature at the top of the edge pedestal. At first glance, this seems surprising, but the high probability of pellets triggering ELMs even when they arrive very soon after a previous ELM indicate that the perturbation introduced by these pellets is sufficient to trigger an ELM even in conditions where the plasma is far from the peeling–ballooning stability limit. Hence it is less surprising that variation in the edge parameter, covered by the experiments described above, only has a moderate effect on this high triggering probability.

The method described in section 3 has allowed us to determine which ELMs are triggered and which are not with good confidence. Using this information, differences between triggered and not triggered ELMs have been studied in [34] and investigations into these differences are continuing.

On a more technical note, the above investigations have shown the benefit of the improvements made to the JET pellet injection system in 2015 and 2017. Not only has a marked improvement been seen in the ELM triggering ability of the pellets which arrive in the plasma, the reliability of getting the pellets through to the plasma has also increased significantly. The latter observation shows the importance of lim-

iting the length and in particular the number of bends in the pellet flight lines to improve pellets survival. As described in section 3, the JET pellet injector is based on compressed air propulsion rather than on a centrifuge. This results in pellets with a significant velocity scatter and hence a large variation in the interval between pellets arriving in the plasma. Despite the resulting irregular ELM behaviour, with a mixture of natural and triggered ELMs, the discharges analysed in this paper have shown good performance without excessive inter-ELM periods, maintaining modest ELM amplitudes and good impurity flushing. This is good news for future machines where flight lines are likely to become longer and where it is likely that, even with a reduced velocity scatter, pellets will not arrive in the plasma at very regular intervals.

The analysis methods developed in this paper are generic and can be used to investigate correlations between any pairs of time sequences. Future applications could include investigations into the triggering of other MHD modes such as NTMs and sawteeth and the triggering/correlation of the onset of other MHD activities.

Acknowledgments

This work has been carried out within the framework of the EUROfusion Consortium and has received funding from the Euratom Research and Training Programme 2014–2018 and 2019–2020 under Grant agreement No. 633053. The views and opinions expressed herein do not necessarily reflect those of the European Commission. This scientific work was partly supported by the Polish Ministry of Science and Higher Education within the framework of the scientific financial resources in the year 2020 allocated for the realization of the international co-financed Project No. 5118/H2020/EURATOM/2020/2.

ORCID iDs

E. Belonohy https://orcid.org/0000-0002-1045-4634
L. Garzotti https://orcid.org/0000-0002-3796-9814
J. Hobirk https://orcid.org/0000-0001-6605-0068
A. Kappatou https://orcid.org/0000-0003-3341-1909
C. Perez von Thun https://orcid.org/0000-0002-1166-2179
M. Valovic https://orcid.org/0000-0002-0855-1056

References

[1] Joffrin E. (The JET team) 2019 Overview of the JET preparation for deuterium–tritium operation with the ITER like-wall *Nucl. Fusion* **59** 112021
[2] Garzotti L. *et al* 2019 Scenario development for *D*–*T* operation at JET *Nucl. Fusion* **59** 076037
[3] ITER Physics Basis Editors *et al 1999 ITER Physics basis Nucl. Fusion* **39** 2137
[4] Beurskens M.N.A. *et al* 2013 The effect of a metal wall on confinement in JET and ASDEX Upgrade *Plasma Phys. Control. Fusion* **55** 124043
[5] Pütterich T. *et al* 2013 Observations on the W-transport in the core plasma of JET and ASDEX Upgrade *Plasma Phys. Control. Fusion* **55** 124036
[6] Dux R. *et al* 2009 Plasma-wall interaction and plasma behaviour in the non-boronised all tungsten ASDEX Upgrade *J. Nucl. Mater.* **390–391** 858–63
[7] Joffrin E. *et al* 2014 First scenario development with the JET new ITER-like wall *Nucl. Fusion* **54** 013011
[8] Lennholm M. *et al* 2015 ELM frequency feedback control on JET *Nucl. Fusion* **55** 06300
[9] Sartori F., Lomas P., Piccolo F. and Zedda M.K. (JET EFDA Contributors) 2008 Synchronous ELM pacing at JET using the vertical stabilisation controller *35th EPS Conf. on Plasma Physics* (Hersonissos, Crete, Greece June 9–13, 2008) http://epsppd.epfl.ch/\ignorespacesHersionissos/pdf/P5_045.pdf
[10] de la Luna E. *et al* 2016 Understanding the physics of ELM pacing via vertical kicks in JET in view of ITER *Nucl. Fusion* **56** 026001
[11] Lennholm M. *et al* 2016 Real-time control of ELM and sawtooth frequencies: similarities and differences *Nucl. Fusion* **56** 016008
[12] Loarte A. *et al* 2014 Progress on the application of ELM control schemes to ITER scenarios from the non-active phase to DT operation *Nucl. Fusion* **54** 033007
[13] Baylor L.R., Parks P.B., Jernigan T.C., Caughman J.B., Combs S.K., Foust C.R., Houlberg W.A., Maruyama S. and Rasmussen D.A. 2007 Pellet fuelling and control of burning plasmas in ITER *Nucl. Fusion* **47** 443
[14] Lang P.T. *et al* 2003 ELM frequency control by continuous small pellet injection in ASDEX Upgrade *Nucl. Fusion* **43** 1110
[15] Lang P.T. *et al* 2008 Investigation of pellet-triggered MHD events in ASDEX Upgrade and JET *Nucl. Fusion* **48** 095007
[16] Baylor L.R. *et al* 2007 Comparison of deuterium pellet injection from different locations on the *D*III-*D* tokamak *Nucl. Fusion* **47** 1598
[17] Géraud A. *et al* 2003 A new pellet injector for steady state fuelling in Tore Supra *Fusion Eng. Des.* **69** 5
[18] Terranova D., Garzotti L., Pégourié B., Nehme H., Frigione D., Martini S., Giovannozzi E. and Tudisco O. 2007 Pellet ablation and mass deposition in FTU: analysis of vertical and low field side injection experiments *Nucl. Fusion* **47** 288
[19] Garzotti L. *et al* 2010 Observation and analysis of pellet material ∇B drift on MAST *Nucl. Fusion* **50** 105002
[20] Huysmans G.T.A., Pamela S., van der Plas E. and Ramet P. 2009 Non-linear MHD simulations of edge localized modes (ELMs) *Plasma Phys. Control. Fusion* **51** 124012
[21] Futatani S. *et al* 2014 Non-linear MHD modelling of ELM triggering by pellet injection in *D*III-*D* and implications for ITER *Nucl. Fusion* **54** 073008
[22] Futatani S., Pamela S., Garzotti L., Huijsmans G.T.A., Hoelzl M., Frigione D. and Lennholm M. 2020 Non-linear magneto-hydrodynamic simulations of pellet triggered edge-localized modes in JET *Nucl. Fusion* **60** 026003
[23] Vinyar I., Geraud A., Wyman M., Dequan L., Lukin A., Umov A., Skoblikov S. and Reznichenko P. 2011 Pellet injectors developed at PELIN for JET, TAE and HL-2A *Fusion Eng. Des.* **86** 2208
[24] Geraud A. *et al* 2007 The JET high frequency pellet injector project *Fusion Eng. Des.* **82** 2183
[25] Géraud A. *et al* 2013 Status of the JET high frequency pellet injector *Fusion Eng. Des.* **88** 1064
[26] Cathey A., Hoelzl M., Lackner K., Huijsmans G.T.A., Dunne M. G., Wolfrum E., Pamela S.J.P., Orain F. and Günter S. 2020 Non-linear extended MHD simulations of type-1 edge localised mode cycles in ASDEX Upgrade and their underlying triggering mechanism *Nucl. Fusion* **60** 124007
[27] Dominski J. and Diallo A. 2020 Identification of a network of nonlinear interactions as a mechanism triggering the onset

of edge localized modes *Plasma Phys. Control. Fusion* **62** 095011
[28] Frigione D. *et al* 2015 Divertor load footprint of ELMs in pellet triggering and pacing experiments at JET *J. Nucl. Mater.* **463** 714
[29] Lang P.T. *et al* 2011 ELM pacing investigations at JET with the new pellet launcher *Nucl. Fusion* **51** 033010
[30] Lang P.T. *et al* 2013 ELM pacing and trigger investigations at JET with the new ITER-like wall *Nucl. Fusion* **53** 073010
[31] Reliability Analytics Corporation, 2010-2020 Reliability Analytics Toolkit https://reliabilityanalyticstoolkit.appspot.com/binomial_confidence_details
[32] Boboc A., Gil C., Pastor P., Spuig P., Edlington T. and Dorling S. 2012 Upgrade of the JET far infrared interferometer diagnostic *Rev. Sci. Instrum.* **83** 10E341
[33] de la Luna E. *et al* 2004 Electron cyclotron emission radiometer upgrade on the Joint European Torus (JET) tokamak *Rev. Sci. Instrum.* **75** 3831
[34] Field A.R. *et al* 2019 The effect of pacing pellets on ELMs, W impurity behaviour and pedestal characteristics in high-power, JET-ILW H-mode plasmas *46th EPS Conf. on Plasma Physics (Milan, Italy, July 8-12 2019) P5.1019* http://ocs.ciemat.es/EPS2019PAP/pdf/P5.1019.pdf